

Article

Discovery of Imidazo[1,2-a]pyridine ethers and Squaramides as Selective and Potent Inhibitors of Mycobacterial Adenosine Triphosphate (ATP) Synthesis

Subramanyam J Tantry, Shankar D. Markad, Vikas Shinde, Jyothi Bhat, Gayathri Balakrishnan, Amit K Gupta, Anisha Ambady, Anandkumar V. Raichurkar, Chaitanyakumar Kedari, Sreevalli Sharma, Naina V Mudugal, Ashwini Narayan, C. N. Naveen Kumar, Robert Nanduri, Sowmya Bharath, Jitendar Reddy, Vijender Panduga, Prabhakar K R, Karthikeyan Kandaswamy, Ramanatha Saralaya, Parvinder Kaur, Neela Dinesh, Supreeth Guptha, Kirsty Rich, David Murray, Helen Plant, Marian Preston, Helen Ashton, Darren Plant, Jarrod Walsh, Peter Alcock, Kathryn Naylor, Matthew Collier, James Whiteaker, Robert E McLaughlin, Meenakshi Mallya, Manoranjan Panda, Suresh Rudrapatna, Vasanthi Ramachandran, Radha K Shandil, Vasan K Sambandamurthy, Khisimu Mdluli, Christopher B. Cooper, Harvey Rubin, Takahiro Yano, Pravin S. Iyer, Shridhar Narayanan, Stefan Kavanagh, Kakoli Mukherjee, V. Balasubramanian, Vinayak P. Hosagrahara, Suresh Solapure, Sudha Ravishankar, and Shahul Hameed P

J. Med. Chem., **Just Accepted Manuscript** • DOI: 10.1021/acs.jmedchem.6b01358 • Publication Date (Web): 11 Jan 2017

Downloaded from <http://pubs.acs.org> on January 11, 2017

Just Accepted

"Just Accepted" manuscripts have been peer-reviewed and accepted for publication. They are posted online prior to technical editing, formatting for publication and author proofing. The American Chemical Society provides "Just Accepted" as a free service to the research community to expedite the dissemination of scientific material as soon as possible after acceptance. "Just Accepted" manuscripts appear in full in PDF format accompanied by an HTML abstract. "Just Accepted" manuscripts have been fully peer reviewed, but should not be considered the official version of record. They are accessible to all readers and citable by the Digital Object Identifier (DOI®). "Just Accepted" is an optional service offered to authors. Therefore, the "Just Accepted" Web site may not include all articles that will be published in the journal. After a manuscript is technically edited and formatted, it will be removed from the "Just Accepted" Web site and published as an ASAP article. Note that technical editing may introduce minor changes to the manuscript text and/or graphics which could affect content, and all legal disclaimers and ethical guidelines that apply to the journal pertain. ACS cannot be held responsible for errors or consequences arising from the use of information contained in these "Just Accepted" manuscripts.

1
2
3
4
5
6
7
8
9
10
11
12
13
14
15
16
17
18
19
20
21
22
23
24
25
26
27
28
29
30
31
32
33
34
35
36
37
38
39
40
41
42
43
44
45
46
47
48
49
50
51
52
53
54
55
56
57
58
59
60

	Ramachandran, Vasanthi; AstraZeneca, Shandil, Radha; Astrazeneca India Pvt Ltd Sambandamurthy, Vasan; AstraZeneca India Pvt Ltd Mdluli, Khisimuzi; TB Alliance, Research Cooper, Christopher; Global Alliance for TB Drug Development (TB Alliance), Rubin, Harvey; University of Pennsylvania School of Med, Department of Medicine Yano, Takahiro; University of Pennsylvania, Medicine Iyer, Pravin; Jubilant Innovation Narayanan, Shridhar; AstraZeneca India Pvt. Ltd., Bioscience Kavanagh, Stefan; AstraZeneca R&D Mukherjee, Kakoli; Integral Biosciences, Balasubramanian , V.; AstraZeneca India Pvt Ltd Hosagrahara, Vinayak; AstraZeneca India Pvt Ltd Solapure, Suresh; AstraZeneca India Pvt Ltd Ravishankar, Sudha; AstraZeneca India Pvt Ltd Hameed P, Shahul; BUGWORKS, MEDICINAL CHEMISTRY

SCHOLARONE™
Manuscripts

Discovery of Imidazo[1,2-a]pyridine ethers and Squaramides as Selective and Potent Inhibitors of Mycobacterial Adenosine Triphosphate (ATP) Synthesis

Subramanyam J. Tantry,^{#†} Shankar D. Markad,^{#†} Vikas Shinde,[†] Jyothi Bhat,[†] Gayathri Balakrishnan,[†] Amit K. Gupta,[†] Anisha Ambady,[†] Anandkumar Raichurkar,[†] Chaitanyakumar Kedari,[†] Sreevalli Sharma,[†] Naina V. Mudugal,[†] Ashwini Narayan,[†] C.N. Naveen Kumar,[†] Robert Nanduri,[†] Sowmya Bharath,[†] Jitendar Reddy,[†] Vijender Panduga,[†] Prabhakar K.R.,[†] Karthikeyan Kandaswamy,[†] Ramanatha Saralaya,[†] Parvinder Kaur,[†] Neela Dinesh,[†] Supreeth Guptha,[†] Kirsty Rich,[§] David Murray,[§] Helen Plant,[§] Marian Preston,[§] Helen Ashton,[§] Darren Plant,[§] Jarrod Walsh,[§] Peter Alcock,[§] Kathryn Naylor,[§] Matthew Collier,[§] James Whiteaker,[‡] Robert E. McLaughlin,[‡] Meenakshi Mallya,[†] Manoranjan Panda,[†] Suresh Rudrapatna,[†] Vasanthi Ramachandran,[†] Radha Shandil,[†] Vasan K. Sambandamurthy,[†] Khisi Mdluli,[§] Christopher B. Cooper,[§] Harvey Rubin,[&] Takahiro Yano,[&] Pravin Iyer,[†] Shridhar Narayanan,[†] Stefan Kavanagh,[§] Kakoli Mukherjee,[†] V. Balasubramanian,[†] Vinayak P. Hosagrahara,[†] Suresh Solapure,[†] Sudha Ravishankar^{†*} Shahul Hameed P,^{†*}

[#]Contributed equally to the work

[†]Innovative Medicines, AstraZeneca India Pvt. Ltd., Bellary Road, Hebbal, Bangalore 560024, India.

[‡]AstraZeneca Infection Innovative Medicines, 35 Gatehouse Drive, Waltham, MA 02451, USA.

[§]AstraZeneca, Alderley Park, Mereside, Macclesfield, Cheshire, UK. SK10 4TG

[§]Global Alliance for TB Drug Development, 40 Wall Street, 24th Floor, New York, NY 10005, USA.

[&]University of Pennsylvania, 111 Clinical Research Building, 415 Curie Boulevard, Philadelphia PA 19104, USA

*Corresponding authors
shahulhameed@bugworksresearch.com
mailsuravi01@gmail.com

KEYWORDS:

Oxidative phosphorylation
ATP synthesis
Imidazo[1,2-a]pyridine ethers
Squaramides

ABSTRACT

The approval of bedaquiline to treat tuberculosis has validated adenosine triphosphate (ATP) synthase as an attractive target to kill *Mycobacterium tuberculosis*. Herein, we report the discovery of two diverse lead series imidazo[1,2-a]pyridine ethers (IPE) and squaramides (SQA) as inhibitors of mycobacterial ATP-synthesis. Through medicinal chemistry exploration, we established a robust structure activity relationship of these two scaffolds resulting in nanomolar potencies in an ATP-synthesis inhibition assay. A biochemical deconvolution cascade suggested cytochrome c oxidase as the potential target of IPE class of molecules, whereas characterization of spontaneous resistant mutants of SQAs unambiguously identified ATP synthase as its molecular target. Absence of cross resistance against bedaquiline resistant mutants suggested a different binding site for SQAs on ATP synthase. Furthermore, SQAs were found to be non-cytotoxic and demonstrated efficacy in a mouse model of tuberculosis infection.

INTRODUCTION

Tuberculosis (TB) continues to be a major health issue with about 1.5 million deaths reported in 2014. One third of the world population is estimated to be exposed to the causative agent *M. tuberculosis*.¹⁻³ Infections with multidrug-resistant (MDR) and extensively drug-resistant (XDR) *M. tuberculosis* strains and co-infection with HIV have further worsened the prospect of controlling this disease.⁴⁻⁶ The prolonged treatment regimen for six months with a combination of four drugs has resulted in poor patient compliance leading to the emergence of MDR and XDR strains of *M. tuberculosis*.⁷⁻⁹ The treatment of MDR or XDR-TB cases with poorly efficacious and not so safe second and third line drugs for 12 to 24 months has further deteriorated the overall success rate of TB treatment.¹⁰ In order to improve the efficacy of TB treatment and to make an impact on the global war against TB, new anti-tubercular agents with a potential to reduce the duration of treatment are required.¹¹ A few existing drugs and several new chemical entities (NCEs) are being profiled in the clinic to test their effectiveness in treating both drug-sensitive and drug-resistant TB cases.¹²⁻¹³ Efforts are in progress to test and optimize new combination of drugs to improve the efficacy of existing drugs and the NCEs emerging out of several ongoing research and development programs.¹⁴⁻¹⁵

Anti-tubercular discovery and development programs select potential drug targets based on a number of criteria such as, (i) novel target or pathway to avoid chances of cross resistance with existing drugs, (ii) essentiality of the target or pathway to the survival of *M. tuberculosis*, (iii) low propensity for development of resistance and (iv) absence of a human homolog to minimize mechanism based toxicity issues.¹⁶ If the chosen target has a human homolog, building in selectivity during chemistry exploration becomes one of the key requirements as non-selective inhibitors may result in acute toxicity issues preventing their clinical utility. The recently

1
2
3 approved drug, bedaquiline to treat drug resistant TB cases is one of the best examples of a
4 selective antimycobacterial agent. It inhibits mycobacterial ATP synthase with a high selectivity
5 index eventhough the process of ATP synthesis is highly conserved across both prokaryotes and
6 eukaryotes.¹⁷⁻¹⁸ The success of bedaquiline in the clinic has resulted in an increased exploration
7 to identify additional inhibitors of mycobacterial ATP synthase and other novel targets and
8 pathways.¹⁹

9
10 ATP synthase is an evolutionarily highly conserved enzyme among prokaryotes and eukaryotes,
11 including humans.²⁰ It supplies cells with bulk of their ATP via the oxidative phosphorylation
12 (Ox-Phos) process and hence essential for cell survival. This multi-subunit complex, the last one
13 in the oxidative phosphorylation pathway, couples the proton motive force to ATP synthesis.²⁰
14
15 Hong *et al.*, have provided a comprehensive review of all known ATP synthase inhibitors and
16 their utility in scientific research.²¹ The well-known inhibitors of ATP synthase, such as
17 dicyclohexyl-carbodiimide (DCCD), oligomycin and venturicidin, which block ATP synthase
18 activity through their interaction with subunit-*c* or subunit-*a/c* interface are poorly selective and
19 are shown to inhibit both bacterial and mitochondrial ATP synthesis.²²⁻²⁴ The lack of selectivity
20 and ensuing toxicity has prevented their use in the clinic. Several studies towards understanding
21 the mechanism of action of ATP synthase inhibitors have led to advances in the methodologies
22 to test for mitochondrial toxicity of drugs in development.²⁵⁻²⁶ In this regard, the discovery of a
23 first in class mycobacterial ATP synthase inhibitor, bedaquiline, from a cell based screen, is
24 noted as a significant contribution towards tuberculosis drug discovery research.¹⁷ This highly
25 selective molecule having the ability to reduce the duration of TB treatment because of its potent
26 activity against both replicating and non-replicating *M. tuberculosis* has indicated the possibility
27 of identifying selective inhibitors of this mechanism.²⁷⁻²⁹ Although FDA approved the use of
28
29
30
31
32
33
34
35
36
37
38
39
40
41
42
43
44
45
46
47
48
49
50
51
52
53
54
55
56
57
58
59
60

1
2
3 bedaquiline for the treatment of tuberculosis, its usage got limited to treat only MDR and XDR-
4
5 TB cases because of the drug-drug interaction risk it carried with the front line drug rifampicin.
6
7 Additionally, its usage in the clinic carries a black-box warning due to the QT-prolongation risk
8
9 observed, leaving the need to discover safer drugs for TB treatment.³⁰ However, the discovery of
10
11 bedaquiline brought to prominence the criticality of ATP synthase for the survival of *M.*
12
13 *tuberculosis* and the possibility of exploring the entire oxidative phosphorylation pathway to
14
15 identify additional inhibitors of this mechanism. Several attempts made in this direction has
16
17 resulted in the identification of a few compounds which inhibit the process of ATP synthesis in
18
19 mycobacteria.³¹⁻³⁷ In order to discover and develop a novel, potent and safe anti-tubercular agent,
20
21 we employed a biochemical screen to identify chemical entities that inhibit the ATP synthesis
22
23 pathway. A membrane based biochemical assay (Myc_ATPS), which measured ATP synthesis
24
25 through the oxidative phosphorylation (Ox-Phos) process, was used to screen AstraZeneca's
26
27 (AZ) corporate compound collection in a high throughput screen (HTS). The high hit rate
28
29 observed in the primary screen led to the development and use of counter screens such as delta
30
31 pH (Δ pH) and mammalian mitochondrial ATP synthesis (SMP_ATPS) assays respectively) in
32
33 order to shortlist specific and selective inhibitors of mycobacterial ATP synthesis pathway.
34
35 Screening of about 900,000 compounds utilizing the cascade presented in **Figure 1** yielded about
36
37 1200 actives with potent IC_{50} ($< 10 \mu M$) and good selectivity. Further hit triage that included
38
39 structure activity relationship (SAR) studies to check the potential for chemical diversification
40
41 and confirmation of activity through re-synthesis of hits led to the identification of multiple
42
43 robust chemical classes. SAR exploration of the potent mycobacterial ATP synthesis inhibitor
44
45 2,4-diaminoquinazolines leading to evolution of 2,4-diaminoquinolines and
46
47 aminopyrazolopyrimidines has been described earlier.³⁷ Here we describe SAR studies and the
48
49
50
51
52
53
54
55
56
57
58
59
60

1
2
3 resulting biological properties of two diverse chemical leads, imidazo[1,2-a]pyridine ethers (IPE)
4
5 and squaramides (SQA) (**Figure 2**), with potent ATP synthesis inhibition and anti-tubercular
6
7 activity. Utility of a biochemical deconvolution cascade and spontaneous mutant generation
8
9 enabled identification of molecular targets of these two scaffolds. A potent and selective
10
11 compound from squaramide series was prioritized to demonstrate *in vivo* proof of principle in a
12
13 mouse model of acute tuberculosis infection.
14
15
16
17
18
19
20
21
22
23
24
25
26
27
28
29
30
31
32
33
34
35
36
37
38
39
40
41
42
43
44
45
46
47
48
49
50
51
52
53
54
55
56
57
58
59
60

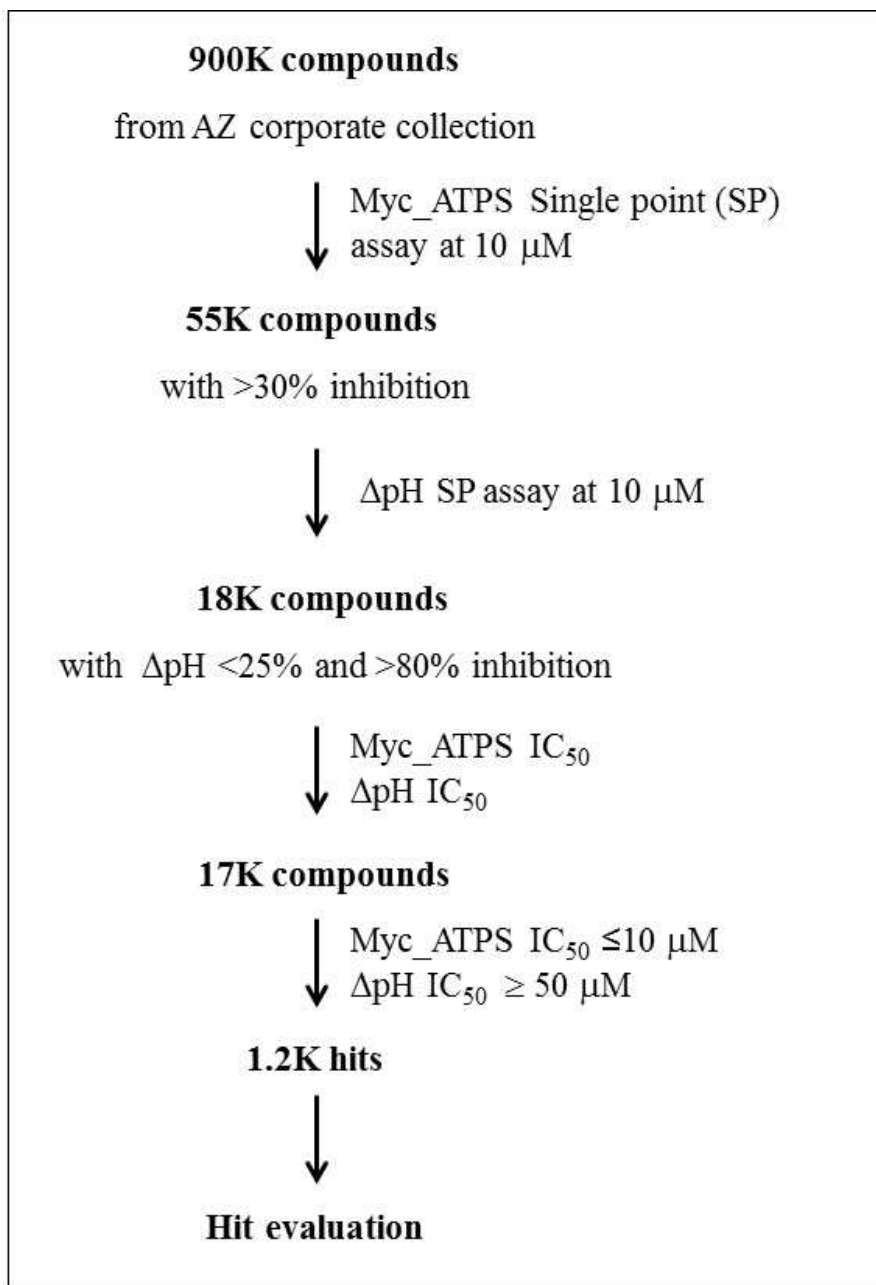
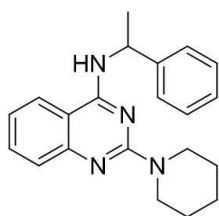
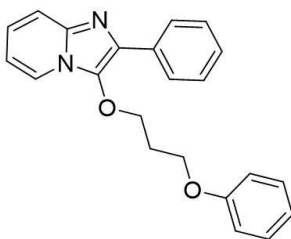
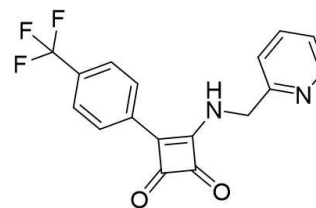


Figure 1. Schematic of HTS and hit triage

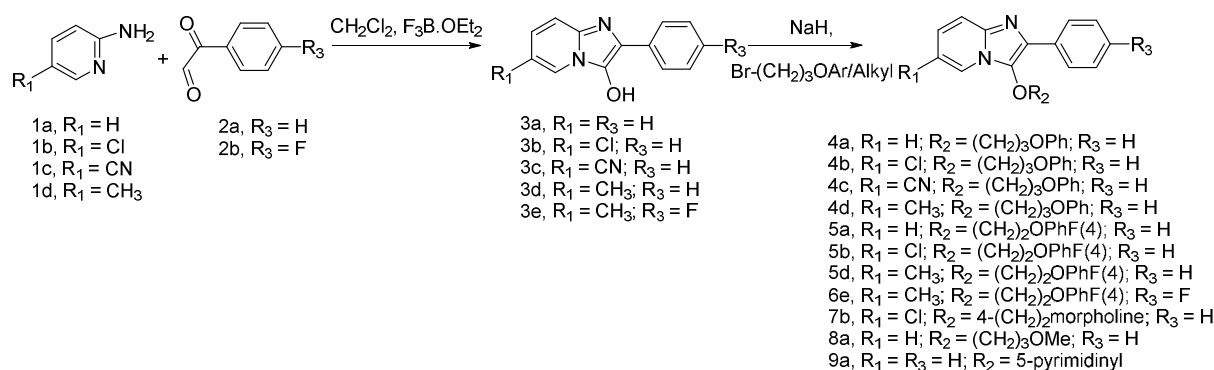
**2,4-Diaminoquinazoline*****Imidazo[1,2-a]pyridine-3-ether****Squaramide****Figure 2.** Prioritized hit series from high throughput screen.

* Published elsewhere.³⁷

CHEMISTRY

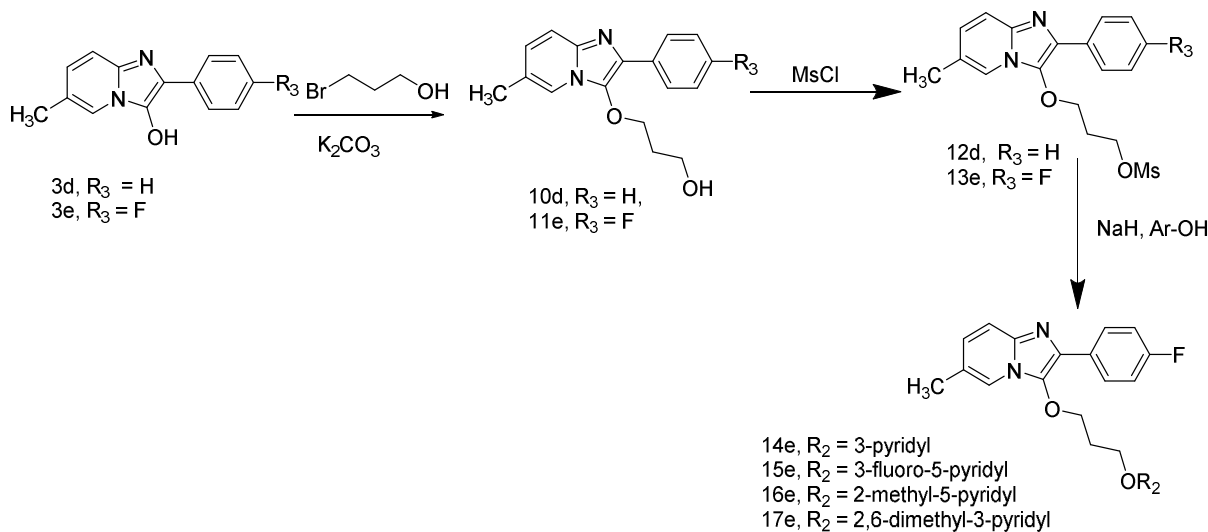
Synthesis of imidazo[1,2-a]pyridine ethers

The condensation of 2-aminopyridines (**1a-1d**) with phenyl glyoxals (**2a, 2b**) in the presence of Lewis acid such as boron trifluoride etherate afforded imidazo[1,2-a]pyridine-3-ols (**3a-3e**) in moderate to excellent yields.³⁸ The required imidazo[1,2-a]pyridine ethers were obtained in good yields by alkylation using suitable alkoxyalkyl or aryloxyalkyl halides in the presence of a base (**Scheme 1**).

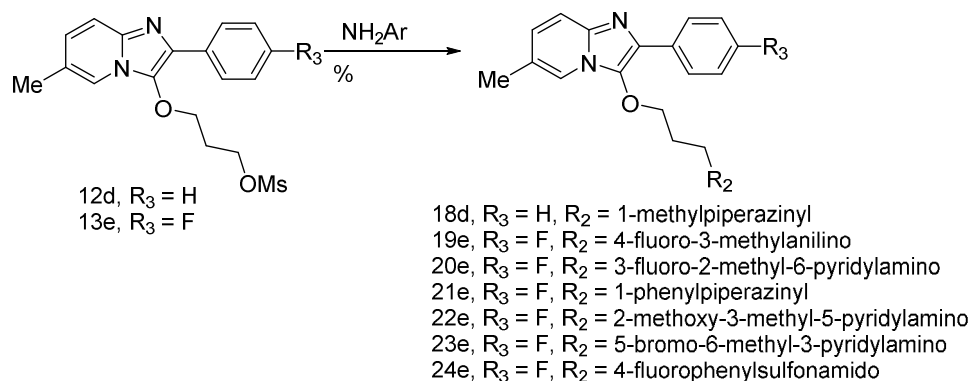


Scheme1. Synthesis of Imidazo[1,2-a]pyridine ethers

In order to introduce a variety of heterocycles at the terminal position of the ether side chain, imidazo[1,2-a]pyridine-3-ols (**3a-3e**) were treated with 3-bromopropanol in the presence of K₂CO₃ as a base to give alcohols (**10d, 11e**). The terminal hydroxy group was converted into its mesyl derivative (**12d, 13e**) under standard conditions (MsCl/NEt₃). Various heteroaryl amines/alcohols were introduced by treating the mesyl derivative with corresponding heteroaryl amines/alcohols in the presence of a base to get imidazo[1,2-a]pyridine-3-ethers (**Schemes 2 and 3**).



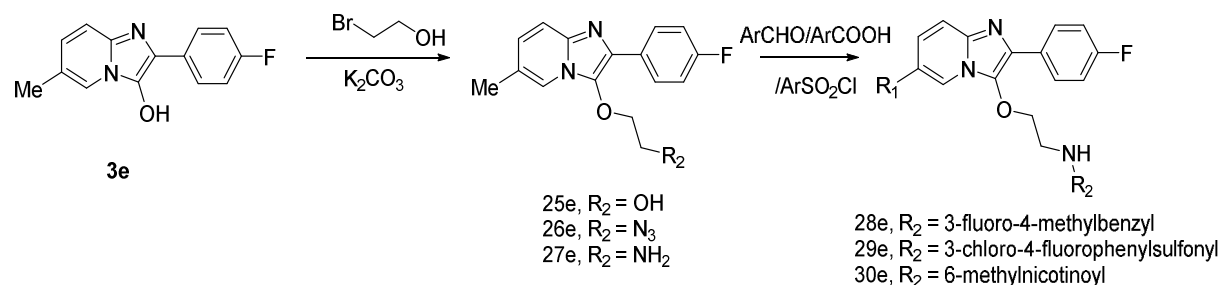
Scheme 2. Synthesis of IPE with heteroaryls



Scheme 3. Synthesis of IPE with heteroarylamines.

The carbon linker of ether side chain was modified to 2 carbon atoms. Imidazo[1,2-a]pyridine-3-ols (**3e**) were treated with 2-bromoethanol in the presence of K_2CO_3 to give alcohol **25e**. The terminal hydroxy group was converted to the corresponding amine by a sequence of reactions; the alcohol was reacted with DPPA to give the azido functionality which in turn was converted to the corresponding amine **27e** under Staudinger reaction conditions. The amine **27e** was converted to the benzylamine derivative **28e** by reductive amination using substituted benzaldehyde. The

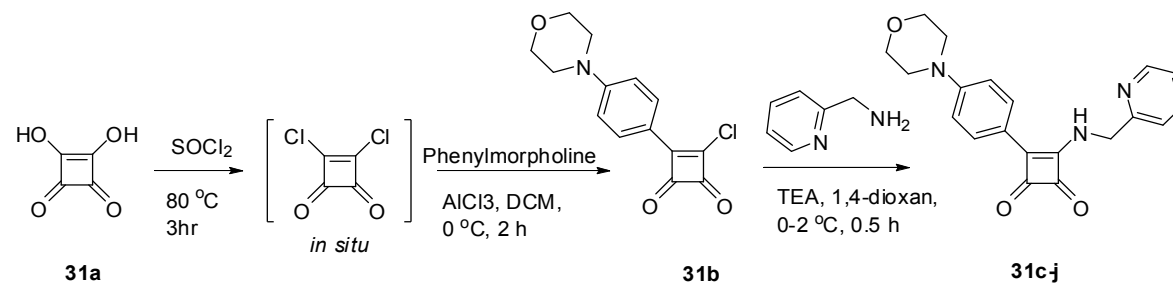
amine **27e** was also converted to sulfonamide **29e** and amide **30e** by treatment with the corresponding sulfonyl chloride and nicotinic acid, respectively (**Scheme 4**).



Scheme 4. Synthesis of IPE amide/sulfonamide

Synthesis of Squaramides:

Scheme 5 depicts the synthetic route followed for the synthesis of squaramides. The dichloride, 3,4-dichloro-3-cyclobutene-1,2-dione was generated *in situ* by treating squaric acid **31a** with thionyl chloride at 0 °C and the resulting dichloride was directly subjected to mono arylation with 4-phenylmorpholine substituted arene in the presence of AlCl_3 as Lewis acid. The exothermic reaction was controlled by slow addition of arene at 0 °C and the subsequent purification resulted in mono chloride **31b** with moderate yield. The mono chloride **31b** could be treated conveniently with various benzylamines in a parallel mode to yield title compounds **31c-j** in moderate yield.



Scheme 5. Synthesis of Squaramides

RESULTS AND DISCUSSION

High throughput screening and hit identification

ATP synthesis assays which used inverted membrane vesicles (IMVs) prepared from either bacterial cytoplasmic membrane or mammalian mitochondrial membrane have been reported previously.^{24, 39-41} The primary screen used in this study (Myc_ATPS assay), derived from the assay reported by Yano et al.,⁴¹ measures the ATP synthesized through the process of oxidative phosphorylation in a luminescence based assay performed with 8 $\mu\text{g/ml}$ of *M. smegmatis* IMVs energized with 150 μM NADH. In a single point high throughput screen at 10 μM concentration, 900,000 compounds from AstraZeneca's corporate compound collection were evaluated for the inhibition of Myc_ATPS assay. This screen yielded inhibitors at a very high hit rate of about 6.1% (**Figure 1**) probably because it also picked up disruptors of proton gradient as ATP synthesis inhibitors in addition to those which inhibited the ATP synthesis pathway. Inhibitors of proton gradient formation would be non-selective and toxic as they can inhibit proton gradient across mammalian mitochondrial membrane as well. To weed-out such compounds, an assay to measure the proton gradient across IMVs was designed (ΔpH assay) by modifying the Myc_ATPS assay wherein substrates of ATP synthase (ADP and P_i) were omitted. The assay was monitored using LysoSensor Green DND-153, a fluorophore linked to a weak base which gets partially protonated at neutral pH and fluoresces at acidic pH with excitation maxima at 485 nm and emission maxima at 523 nm.⁴² The output of primary screen, 55K actives, when screened at 10 μM in a single point ΔpH assay resulted in the selection of 18K compounds which were taken for dose response studies to determine IC_{50} in both the Myc_ATPS and ΔpH assays (**Figure 1**). Minimum inhibitory concentration (MIC) for *M. tuberculosis* (minimum

concentration required to inhibit the growth by 80%) and mammalian cell lines like THP1 and/or A549 (MMIC – minimum concentration required to inhibit the mammalian cell proliferation by 50%) were determined with 1200 compounds having Myc_ATPS $IC_{50} \leq 10 \mu M$ and ΔpH $IC_{50} \geq 50 \mu M$. In addition, evaluation of identified chemical series for physicochemical properties and chemical tractability for SAR expansion led to choosing two scaffolds for re-synthesis, confirmation of activities and follow up SAR (**Figure 2**).

Structure activity relationship (SAR) studies of imidazo[1,2-a]pyridine ethers

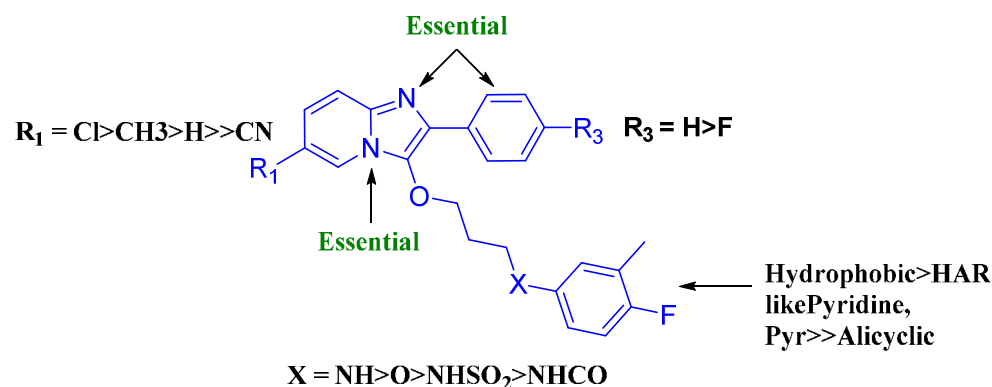


Figure 3. SAR for imidazo[1,2-a]pyridine ethers

All compounds synthesized during SAR studies were tested in the mycobacterial ATP synthesis assay (Myc_ATPS IC_{50}) and in the anti-mycobacterial assay (*M. tuberculosis* MIC) for assessing the potency, as well as in the mammalian cell proliferation assay (MMIC) for assessing cytotoxicity. Cytotoxicity index, the ratio of MMIC to MIC guided the SAR studies towards the synthesis of selective inhibitors.

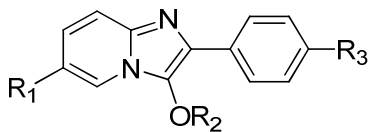
The generic SAR for IPE series is depicted in **Figure 3**. In general, the position of bridgehead nitrogen in [1,2-a] format and the presence of a phenyl ring directly attached to the imidazole portion of IPE core are essential for retaining biological activity (both ATP synthesis inhibition and *M. tuberculosis* MIC). Chloro or methyl substitution at R1 position gave best potency,

whereas H preferred over F at R3 position for improved potency. The terminal aryl linkage through –NH– or –O– at X provided the best potency, whereas the amide (–NHCO–) and sulphonamide (–NH₂SO₂–) linkages were found to be weakly active. The substituted phenyl is preferred over hetero aromatic rings like pyridine or pyrimidine at the side chain terminal ring system for maintaining best potency. A detailed SAR for IPE series is presented in tables 1- 4.

The SAR of IPE series was studied by incorporating various substitutions on imidazo[1,2-a]pyridine followed by optimization of the ether side chain. The unsubstituted compound **4a** showed ATP synthesis IC₅₀ of 0.13 μM and *M. tuberculosis* MIC of 1.6 μM in the enzymatic and cellular assays, respectively. Introduction of an electron withdrawing and hydrophobic chloro substitution at 6-position of the imidazo[1,2-a]pyridine gave compound **4b** that showed nearly eight-fold improvement in ATP synthesis inhibition and 3-fold improvement in cellular potency compared to the unsubstituted compound **4a**. In contrast, electron withdrawing and hydrophilic cyano-substituted compound **4c** lost activity completely. This data indicated that the hydrophobic substituents are more favored in the ring for potency improvement. In order to expand the SAR and confirm the hydrophobic group requirement for activity, we made methyl substituted compound **4d**, which was found to be equipotent to the chloro substituted compound and thus reinforced the requirement of hydrophobic substituents for potency. There was no significant drop in potency when the spacer length of ether side chain was shortened from 5 to 4 atoms as demonstrated by **5a**, **5b**, **5d** and **6d**; however, aliphatic and alicyclic groups, compounds **8a** and **7b** respectively, were not tolerated. Compounds from the first set of design make test and analyze (DMTA) cycle showed high *in vitro* metabolic clearance due to the presence of metabolic soft spots. Introduction of metabolically stable fluoro substitution at para position of the distal phenyl ring (**6d**) resulted in a 2-fold improvement in reducing rat *in vitro* metabolic CL_{int} without

compromising the potency, e.g., compound **5d** (Rat hepatic CL_{int} = 394.6 μL/min/10⁶ cells) vs. **6d** (Rat hepatic CL_{int} = 186.6 μL/min/10⁶ cells).

Table 1. SAR of substituted imidazo[1,2-a]pyridine ethers



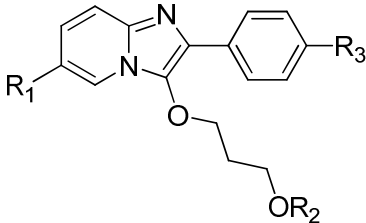
^a No.	R1	R2	R3	^b ATPS IC ₅₀ (μM)	^c <i>Mtb</i> MIC (μM)	^d C- Index	LogD
4a	H		H	0.13	1.6	>62	>5
4b	Cl		H	<0.02	<0.5	>144	>4.3
4c	CN		H	>100	>250	~ 0.4	>4.2
4d	CH ₃		H	0.03	<0.5	128	>4.3
5a	H		H	0.08	<0.8	74	>4.7
5b	Cl		H	0.04	<1	>18.5	>4.1
5d	CH ₃		H	0.05	<1.0	>30.4	>5.1
6d	CH ₃		F	0.02	3.1	6	>5.2
7b	Cl		H	36.1	>200	~0.5	3.3
8a	H		H	18.9	>15	~7	3.3

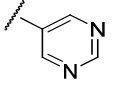
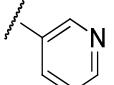
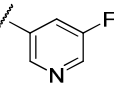
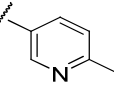
^acompound number; ^bMyc_ATPS IC₅₀; ^c*M. tuberculosis* MIC; ^dCytotoxicity index.

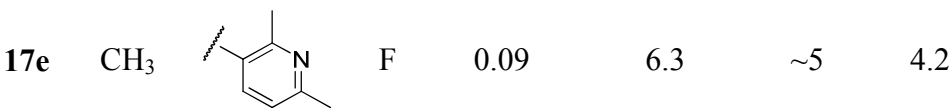
Optimization of the ether side chain

The ether side chain was optimized by keeping 2-(4-fluorophenyl)-6-methyl substitution constant on the imidazo[1,2-a]pyridine ethers. Changing the distal phenyl to pyrimidine (**13a**) on the terminal position of ether side chain resulted in reduced LogD and improved solubility (445 μ M), but the compound lost potency significantly. However, replacing phenyl with 3-pyridyl (**14e**) ring was well tolerated, but the compound showed low cytotoxicity index. While the introduction of methyl or fluoro substitution on distal pyridyl ring reduced the cytotoxicity, solubility did not improve for the pyridyl and phenyl substituted compounds due to high Log D.

Table 2. SAR of ether side chain of imidazo[1,2-a]pyridine ethers



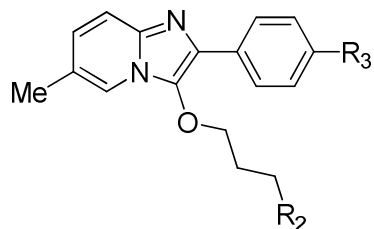
^a No.	R1	R2	R3	^b ATPS IC ₅₀ (μ M)	^c <i>Mtb</i> MIC (μ M)	^d C- index	LogD
13a	H		H	5.6	6.9	14.5	2.9
14e	CH ₃		F	0.16	<0.9	>8	3.9
15e	CH ₃		F	0.06	<0.6	>39	4.1
16e	CH ₃		F	<0.02	<0.8	>11	4.1



^aCompound number; ^bMyc_ATPS IC₅₀; ^c*M. tuberculosis* MIC; ^dCytotoxicity index.

To lower the lipophilicity and demonstrate a solubility handle for the series, the terminal oxygen atom was modified to basic nitrogen through pKa modulation. The terminal ether of the side chain modification with 1-methylpiperazine showed excellent improvement in solubility (674 μM) with diminished ATP synthesis inhibitory activity (compound **4d** vs. **18d**). However, 1-phenylpiperazine substitution was tolerated (IC₅₀ = 0.05 μM) indicating the criticality of the terminal aryl/heteroaryl substitution for the activity. Further modification of distal phenyl piperazine into suitably substituted aniline/pyridine amines retained the potency (compounds **20e**, **22e** and **23e**). Replacement of the terminal arylamine group by sulfonamide showed moderate potency (**24e**). Compound **19e** with 4-Flouoro-3-methylphenyl group was found to be the best substitution for IPE with IC₅₀ = 5 nM; MIC = 31 nM and also had a 1000-fold cytotoxicity index.

Table 3. SAR of ether side chain of imidazo[1,2-a]pyridine ethers



^a No.	R2	R3	^b ATPS IC ₅₀ (μM)	^c <i>Mtb</i> MIC (μM)	^d C- index	LogD
18d		H	6.4	>200	<0.2	2.4
19e		F	0.005	0.03	1050	4.1
20e		F	0.06	<0.5	>113	3.9
21e		F	0.05	<0.8	>125	4.0
22e		F	0.08	<0.8	>125	4.2
23e		F	0.21	0.8	1.4	3.8
24e		F	0.7	1.6	ND	3.9

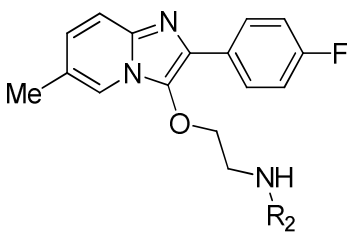
^aCompound number; ^bMyc_ATPS IC₅₀; ^c*M. tuberculosis* MIC; ^dCytotoxicity index, ND: Not Done

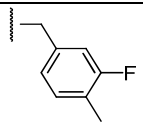
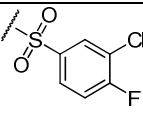
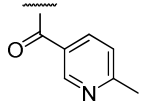
The ether side chain was further optimized by changing the 3 carbon linker to 2 carbon linker.

The 3-fluoro-4-methylbenzyl substitution **28e** was tolerated with IC₅₀ = 0.07 μM; MIC = 0.6 μM

with improved solubility of 22 μM compared to **19e** solubility of $<1\ \mu\text{M}$. The sulfonamide **29e** was moderately active, whereas the nicotinamide compound **30e** was found to be weakly active against ATP synthesis inhibition.

Table 4. SAR of the chain length of imidazo[1,2-a]pyridine ethers



^a No.	R2	^b ATPS IC ₅₀ (μM)	^c <i>Mtb</i> MIC (μM)	^d C-index	LogD
28e		0.07	0.6	>167	4.0
29e		0.4	3.1	ND	4.1
30e		7.2	>200	ND	3.4

^aCompound number; ^bMyc_ATPS IC₅₀; ^c*M. tuberculosis* MIC; ^dCytotoxicity index, ND: Not Done.

In general, as shown in **figure 4**, the anti-tubercular potency (pMIC) correlated well with ATP synthesis inhibition potency (pIC₅₀) for the IPE series suggesting that the inhibition of *M. tuberculosis* growth was primarily through inhibition of ATP synthesis.

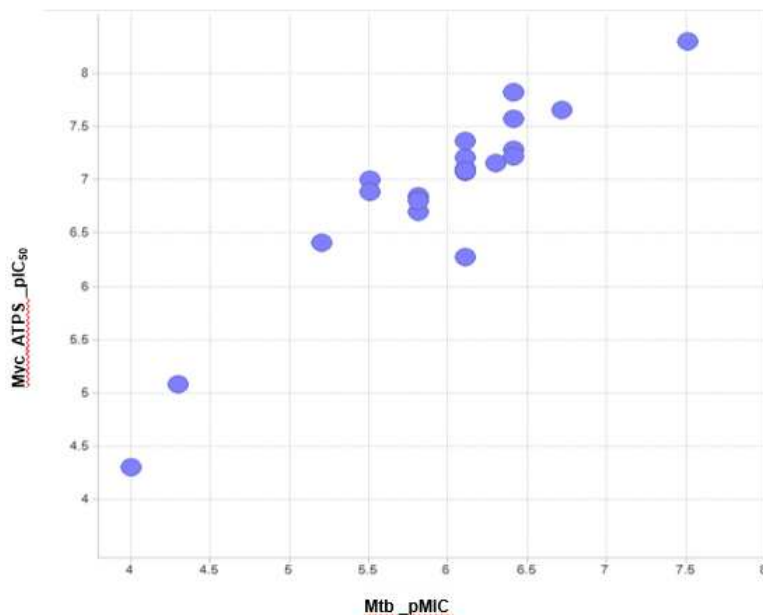


Figure 4. Scatter plot of pIC_{50} ($-\log(\text{Myc_ATPS } IC_{50})$) vs $pMIC$ ($-\log(\text{Mtb_MIC})$).

Mtb: *M. tuberculosis*

Structure activity relationship of squaramides series

One of the initial hits, **31c**, belonging to squaramide series had demonstrated reasonable potency both at enzymatic and cellular levels. In an attempt to understand the SAR (**Figure 5**) and improve the cellular potency (*M. tuberculosis* MIC), few analogues were synthesized as summarized in **table 5**.

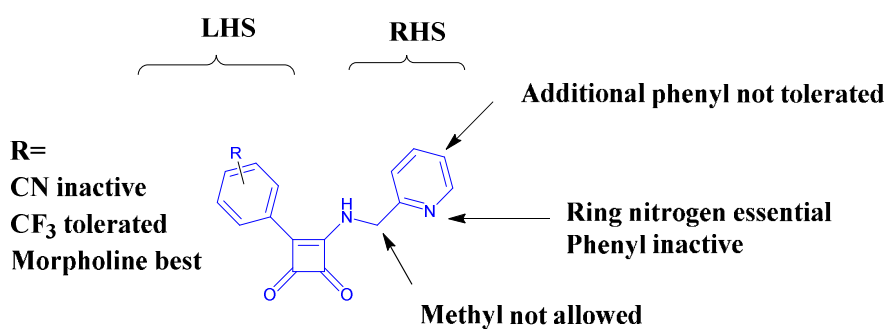
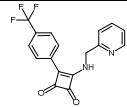
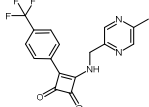
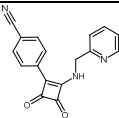
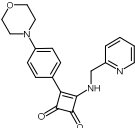
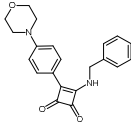
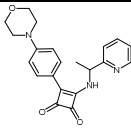
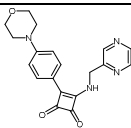
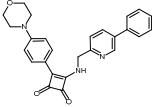


Figure 5. Squaramide SAR

Table 5: SAR of squaramides

^a No.	Structure	^b ATPS IC ₅₀ (μM)	^c <i>Mtb</i> MIC (μM)
31c		0.3	6.2
31d		8.4	50
31e		66.6	100
31f		0.03	0.5
31g		>100	>100
31h		>25	>100
31i		0.77	3.12
31j		9.5	>100

^aCompound number; ^bMyc_ATPS IC₅₀; ^c*M. tuberculosis* MIC

Limited SAR exploration around squaramide series suggested that 2-pyridylmethyl substitution on right hand side (RHS) of the molecule is critical for achieving good enzyme and cellular potency, whereas on the left hand side (LHS) of the squaramide core, morpholino phenyl substitution gave the best activity. Replacement of the hydrophobic electron withdrawing CF₃ group with hydrophilic cyano substitution on phenyl ring weakened the enzyme potency >200-fold and cellular potency by 15-fold (compound **31c** vs **31e**). Further, modification of CF₃ to morpholino ring improved both enzyme and cellular potency >10-fold compared to the initial hit (**31c** vs **31f**). Improved potency observed with compound **31f** may be due to the increased size and the additional hydrogen bonding potential of morpholino ring. Having observed best potency with **31f**, we fixed morpholino phenyl substitution and started exploring SAR on the amino group substitution. Replacement of 2-pyridyl methyl with pyrazine ring weakened the enzyme potency by 25-fold, whereas replacement with benzyl group completely abolished the enzyme potency (compounds **31f** vs **31g** and **31i**). This modification indicated that the pyridine nitrogen may be involved in critical hydrogen bonding interaction with the enzyme and thus essential for maintaining good enzyme potency. An attempt towards restricting the flexibility of amino methyl linker by alpha methyl substitution **31h** and extending the molecule by adding a phenyl group **31j** made the resulting molecule inactive. These results indicated that there may be limited space available for extending the molecule from the aromatic ring attached to amino portion of squaramide core.

IPE and SQA are specific and selective inhibitors of mycobacterial ATP synthesis

SAR studies established that the compounds in the two novel series inhibited mycobacterial ATP synthesis. However, it was necessary to ensure that the inhibition observed is not due to disruption of the proton gradient, an essential event in the process of ATP synthesis or due to

non-specific perturbation of the membrane (IMV). During SAR studies, selected sets of compounds from each of the two series were again profiled in the Δ pH assay to eliminate the potential proton gradient disruptors and also in a membrane damage assay to eliminate compounds which would perturb integrity of the mycobacterial membrane. While the Δ pH assay was a modification of the Myc_ATPS assay, membrane damage assay was an adaptation from an assay reported earlier for *Staphylococcus aureus*.⁴³ *Mycobacterium bovis* BCG (BCG) was used as a surrogate in the cell based membrane damage assay due to good translation of MIC between BCG and *M. tuberculosis* and the ease of handling BCG. A mid-log phase BCG culture was pre-loaded with the fluorophore 3, 3'- Diethyloxacarbocyanine iodide (DiOC₂) before exposure to compound. Stacked DiOC₂ molecules exhibit a red shift in the emission wavelength at 600 nm upon exposure to bacterial cells and an increase in fluorescence is correlated with an increase in membrane potential.⁴³ Compounds like CCCP which dissipate membrane potential served as a positive control in this assay. We found all the compounds tested had an IC₅₀ of >100 μ M in the membrane damage assay with a 100-1000X window with the IC₅₀ in the Myc_ATPS assay (**Table S1**). As the process of ATP synthesis is well conserved across both prokaryotes and eukaryotes, to measure the selectivity with which the compounds were inhibiting mycobacterial ATP synthesis over mammalian mitochondrial ATP synthesis, compounds were routinely tested in a mammalian mitochondrial ATP synthesis assay (SMP_ATPS) which used sub-mitochondrial particles (SMP) from bovine heart mitochondria as a source of mitochondrial Ox-Phos components. The ratio of IC₅₀ in the SMP_ATPS assay to that in Myc_ATPS assay (selectivity index) helped in designing molecules during each design-make-test-analyze (DMTA) cycle. As seen in **Table S1**, a good selectivity index for compounds from SQA and IPE series suggested them to be selective inhibitors of mycobacterial ATP synthesis. Additionally, all compounds

1
2
3 were also tested for cytotoxicity either in A549 or THP1 cell line (MMIC) to get a measure of
4
5 cytotoxicity index (ratio of MMIC to MIC) at the cellular level with respect to *M. tuberculosis*
6
7 MIC. The compounds were also found to selectively inhibit mycobacterial growth as they failed
8
9 to inhibit the growth of two Gram positive and two Gram negative organisms tested in a
10
11 preliminary MIC assay (**Table S2**). Together, the data presented in **Tables S1 and S2** indicated
12
13 that compounds of IPE and SQA series were specific and selective inhibitors of mycobacterial
14
15 ATP synthesis.
16
17
18
19

20 21 **Mode of action of SQA and IPE compounds**

22 23 **SQA resistant mutation mapped to subunits-*a* and *c* of *M. tuberculosis* ATP synthase**

24
25 After the confirmation that the IPE and SQA compounds specifically and selectively inhibited
26
27 mycobacterial ATP synthesis pathway, we wanted to further narrow down their mechanism of
28
29 action to a particular component in the pathway. In order to identify the exact molecular target
30
31 getting inhibited by the SQA and the IPE series compounds, attempts were made to raise
32
33 spontaneous resistant mutants against compound **19e** from IPE series and **31f** from SQA series.
34
35
36
37 *M. tuberculosis* cells were plated on 7H10 plates supplemented with 4, 8 and 16-fold MIC of **31f**
38
39 and upto 100X MIC of **19e**. While resistant mutants could not be raised against **19e** probably due
40
41 to its bacteriostatic property (**Table S3**) and poor solubility, mutant colonies were obtained at a
42
43 frequency of 10^{-8} for **31f**. Two colonies from the 4X MIC plate and three from the 8X MIC plate
44
45 of **31f** were profiled for resistant phenotype against key compounds from the SQA series and a
46
47 few reference inhibitors. All the colonies tested were resistant to all the squaramide compounds
48
49 (**31c**, **31i**, **31f**) with MIC shifting up >8-fold, while the MIC shift for reference inhibitors like
50
51 isoniazid and rifampicin were less than or equal to 4-fold (**Table 6**).
52
53
54
55
56
57
58
59
60

Table 6: MIC modulation in SQA resistant mutants

Series	Compound	<i>Mtb</i> MIC	MIC (μM) in 31f resistant mutants				
		μM	4.1	4.2	8.1	8.2	8.4
SQA	31c	6.3	>100	>100	100	100	>100
	31f	0.8	>100	>100	100	>100	>100
	31i	12.5	>100	>100	>100	>100	>100
Reference	Rifampicin	0.004	0.008	0.008	0.016	0.004	0.008
	Isoniazid	0.02	0.03	0.02	0.03	0.02	0.03

Mtb: *M. tuberculosis* H37Rv

Genomic DNA prepared from all these five colonies were analysed by whole genome sequencing for single nucleotide polymorphism (SNP). A number of observed SNPs were either in non-essential genes or occurred at very low frequency (data not shown). Only two significant SNPs occurred at high frequency in known essential genes. **Table S4** summarizes these SNPs wherein three of the mutations (K179N) mapped to subunit-*a* (encoded by *atpB*) of ATP synthase and two (D28N) to the subunit-*c* (encoded by *atpE*) of ATP synthase. SNP at Asp 28th position of subunit-*c* has been observed previously with bedaquiline mutants of *M. tuberculosis*, *M. fortuitum* and *M. abscessus*, with the *M. tuberculosis* mutants exhibiting more than or equal to 16-fold MIC up-shift.⁴⁴ SQA compounds were also selective like bedaquiline with respect to the inhibition of mycobacterial ATP synthesis. Good selectivity index observed with SQA compounds in the SMP_ATPS assay over that of Myc_ATPS assay could now be explained based on the differences in the amino acid present at this particular position (28th amino acid) between *M. tuberculosis* and mammalian mitochondrial ATP synthase subunit-*c*, Asp and Ile

1
2
3 respectively (data not shown). Unlike the case with SQA, no mutations in the *atpB* gene
4
5 encoding subunit-*a* of Fo component of ATP synthase has been reported earlier for
6
7 bedaquiline.⁴⁴⁻⁴⁵
8
9

11 **Proposed binding mode of SQA**

12
13 Bacterial ATP synthases have a lipophilic intramembrane portion (Fo) with subunit composition
14
15 of $a_1b_2c_{10-15}$ and a polar ATP-binding region (F₁) consisting of subunits $\alpha_3\beta_3\gamma\delta\epsilon$ that extends into
16
17 the cytoplasm.
18
19

20
21 Recent breakthrough in crystallographic efforts⁴⁶ revealed that bedaquiline primarily binds at the
22
23 interface of two subunit-*c* chains (chain A and chain B) of ATP synthase. Binding of bedaquiline
24
25 at this site causes a conformational change of Phe-69 of subunit-*c* providing a hydrophobic space
26
27 for its quinoline moiety. Further, carbonyl group of Glu-65 backbone anchors the bedaquiline's
28
29 hydroxyl group through water mediated H-bond. The binding of bedaquiline, thus plugs the
30
31 rotation of subunit-*c* chains (**Figure 6A**). Till date all the bedaquiline resistant *M. tuberculosis*
32
33 strains have the mutations mapped to only subunit-*c* and none to any other subunit of ATP
34
35 synthase,^{7,44} suggesting that bedaquiline primarily binds at the interface of two subunit-*c* chains
36
37 (chain A and chain B) and plugs their rotation.
38
39
40
41

42
43 SNP studies of SQA resistant strain suggested that both subunits -*c* and -*a* play a critical role in
44
45 the binding of SQA compounds to ATP synthase. This encouraged us to study the possible
46
47 binding modes of SQA to ATP synthase through molecular modeling and generate hypotheses
48
49 for the observed SAR.
50
51
52
53
54
55
56
57
58
59
60

Docking studies with SQA class of ATP synthase inhibitors

In order to understand the plausible mode of binding and a rationale for the observed SAR for SQA compounds, we performed docking studies of SQA molecules over the a/c-ring interface construct of *M. tuberculosis* ATP synthase. This a/c-ring construct was prepared using crystal structure of subunit-*c* ring bound with bedaquiline⁴⁶ and the previously reported homology model of subunit-*a*,³⁷ which was developed using *E. coli* ATP synthase (PDB ID : 1C17) as template.

SQA compounds were subjected to the InducedFit docking algorithm⁴⁷ of the Schrodinger software package⁴⁸ where the amino acid residues of proteins were also allowed to move freely along with docked ligand. The receptor grid (active site of the protein) was generated using the co-crystallized structure of bedaquiline. The induced fit docking resulted in multiple binding poses. Post docking analysis was performed to select the best binding pose where the ligands were first clustered based on their common interactions with residues followed by docking score. The highest docking score conformation among the largest populated cluster sharing common interactions was selected as the best binding pose for these ligands.

The binding site interaction of the most active squaramide **31f** in the a/c-ring interface of *M. tuberculosis* ATP synthase model is shown in **Figure 6B**. Pyridine ring and its nitrogen atom of **31f** was found to form π - π interaction and H-bond with Arg-186 of subunit-*a* respectively. Furthermore morpholine oxygen atom was observed to interact with Phe-69 of subunit-*c* through water mediated H-bond. These H-bond contacts seem to provide firm anchoring to the molecule at both ends. This diagonal binding of compound **31f** at the interface of two subunit-*c* chains (chain A and chain B) and subunit-*a* of ATP synthase most likely plugs the rotation process of

subunit-*c* resulting in the inhibition of ATP synthesis and can thus explain its high potency ($IC_{50} = 0.03 \mu M$).

The predicted binding mode of compounds **31c** and **31i** (Figures 6C and 6D respectively) revealed that these molecules followed the same binding pattern as compound **31f**. Replacement of the morpholino group of **31f** with trifluoro functional group in compound **31c** did not alter the binding pattern of pyridine group at the a/c interface as compared to **31f**. However, low potency ($IC_{50} = 0.3 \mu M$) observed with **31c** could be due to the inability of trifluoro group to make any H-bond at the interface of two chains of subunit-*c* compared to the morpholino group of compound **31f** (Figure 6B) which is required to anchor the molecule.

The predicted binding mode of compound **31i** revealed that pyrazine ring and the nitrogen at 4' position also makes H-bond contact with Arg-186 of subunit-*a* resulting in a shift of pyrazine ring towards subunit-*c*. However H-bond interaction of pyrazine ring linked -CH₂ group with Ile-59 residue moves the morpholino group away from the water molecule making it unavailable to make the H-bond (Figure 6D). This results in making the molecule less efficient to plug the interface of 'a' and 'c' subunits and thereby leading to lesser potency ($IC_{50} = 0.77 \mu M$) than **31f**. These observations not only indicated that squaramide compounds occupy a different binding site than bedaquiline to plug the rotation process but also explained the variation in the ATP synthesis inhibitory activity among the SQA inhibitors. (pdb files of mycobacterial ATP synthase models with respective ligands are presented in the supporting information file **img.pdb.zip**).

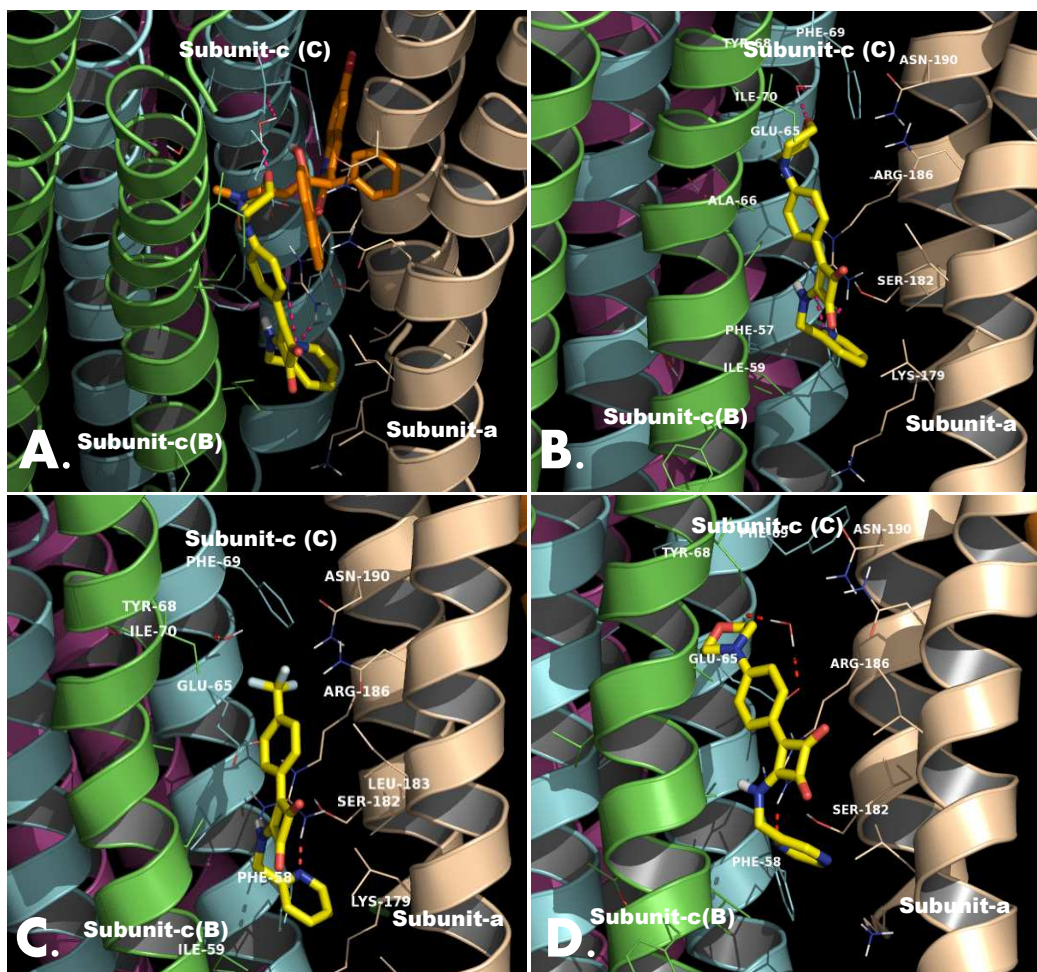


Figure 6. Binding mode of inhibitors at the *M. tuberculosis* ATP synthase binding site. **A.** Compound **31f** superimposed with the crystal structure of bedaquiline; **B.** Compound **31f**; **C.** Compound **31c**; and **D.** Compound **31i**. Helices in green and cyan color are chains B and C of *c*-subunit, respectively, whereas helix in wheat color is subunit-*a* of F₀ particle of ATP synthase.

Imidazo[1,2-*a*]pyridine ethers inhibit cytochrome c oxidase

The Myc_ATPS assay identified imidazo[1,2-*a*]pyridine ethers as potent inhibitors of mycobacterial ATP synthesis. The inability to obtain spontaneous resistant mutants of IPE compounds led us to explore other avenues to identify the molecular target getting inhibited by

these compounds. We utilized a biochemical deconvolution scheme (**Figure 7**) to identify the target site of imidazo[1,2-a]pyridine ethers within the Ox-Phos pathway.

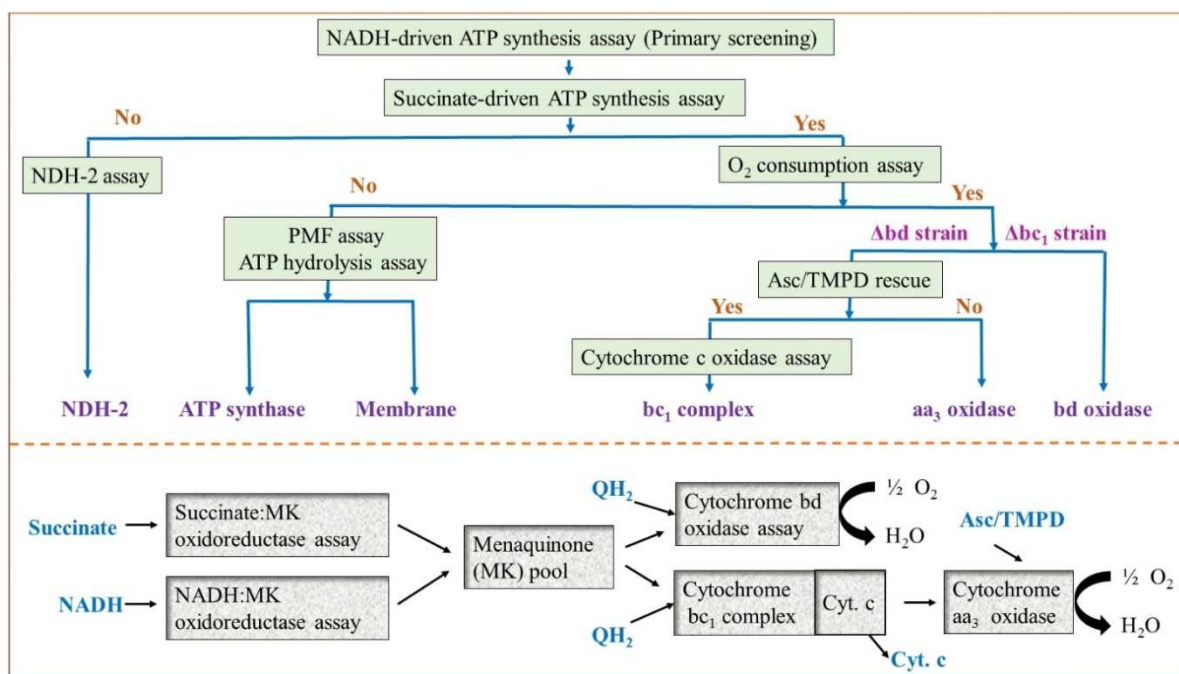


Figure 7. Biochemical deconvolution scheme for the identification of site of inhibition.

Lower portion of the schematic represents mycobacterial Ox-Phos pathway. Top portion of the schematic represents the biochemical deconvolution scheme followed. MK: Menaquinone; QH_2 : Reduced cytochrome c; Asc/TMPD: Ascorbate/N,N,N',N'-tetramethyl-p-phenylenediamine; PMF: Proton Motive Force.

Target site de-convolution involved several steps to arrive at the potential target (**Figure 7**). It started with ruling out that the IPEs were not inhibitors of either NADH:menaquinone (NADH:MK) oxidoreductase (NDH-2) or succinate:menaquinone (Succinate:MK) oxidoreductase (SDH) by performing Myc_ATPS assay using NADH or Succinate as initial electron donors in two parallel assays. Compounds which inhibited the Myc_ATPS assay with

equal potency whether NADH or succinate was used as initial electron donor would be considered to inhibit an Ox-Phos component beyond these two enzymes. We observed that all the IPE compounds tested had similar IC_{50} s in both the assays which was reflected in the ratio of ~ 1 calculated from the individual IC_{50} values (**Table 7**). Bedaquiline, an inhibitor of mycobacterial ATP synthase which was used as a reference inhibitor in these assays exhibited a ratio of about 1. The next set of assays utilized inverted membrane vesicles prepared from *M. smegmatis* strains lacking either cytochrome bc₁ complex (Δ cyt-bc₁) or cytochrome bd oxidase (Δ cyt-bd) or cytochrome aa₃ oxidase (Δ cyt-aa₃). In mycobacteria, cytochrome c oxidase (bc₁-aa₃ super complex) and cytochrome bd oxidase function as terminal oxidases in the electron transport chain. While cytochrome c oxidase is the most favored in aerobic conditions, cytochrome bd oxidase accepts electrons in low oxygen conditions. Additionally, in *M. smegmatis*, cytochrome bd oxidase was observed to compensate the absence of cytochrome c oxidase.⁴¹ Inhibitors of these cytochrome oxidases can therefore be identified in Myc_ATPS assay or oxygen consumption assay using membranes which lack one or the other terminal oxidases. In the cascade, compounds which fail to inhibit either of the cytochrome oxidases in addition to not inhibiting either NDH-2 or SDH were considered to inhibit ATP synthase. As shown in **Table 7**, the representative set of compounds from this series exhibited a loss in potency of at least 20-fold in the NADH driven Myc_ATPS assay which used the Δ cyt-bc₁ membrane as compared to the potency in the same assay which used wild-type membrane suggesting the potential target site as cytochrome c oxidase (cytochrome bc₁-aa₃ super complex).

Table 7: Biochemical deconvolution

Inhibitor	^a Ratio of IC _{50s}	^b Ratio of IC _{50s}	^c Inhibition of O ₂ consumption	^d Inhibition of O ₂ consumption
4d	1.3	35	Yes	No
5b	1.1	165	Yes	No
5d	1.2	26	Yes	No
6d	0.7	82	Yes	No
13a	0.7	24	Yes	No
Bedaquiline	1.5	2	No	No

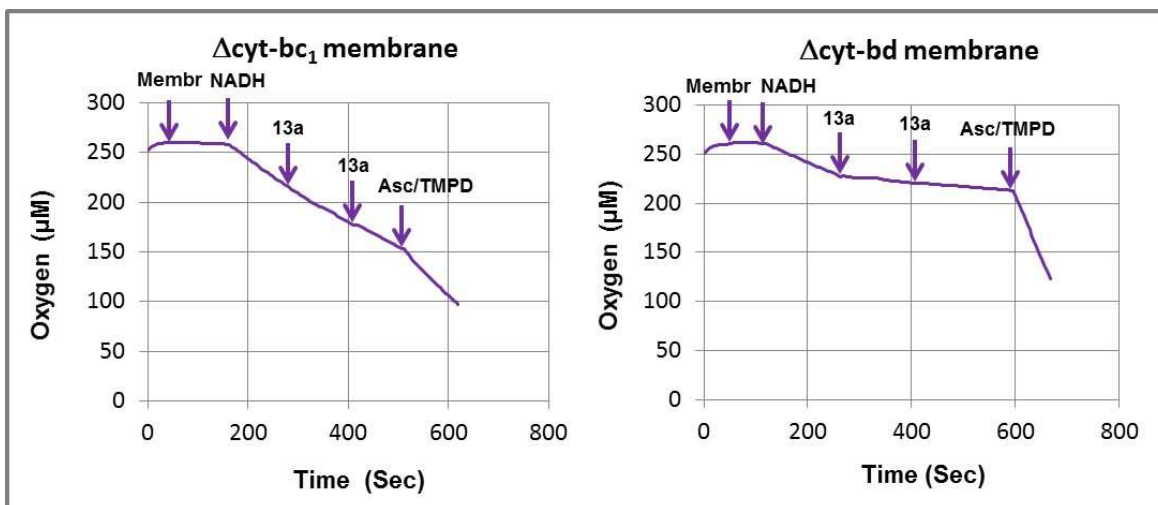
^a Ratio of IC₅₀ in NADH driven to Succinate driven Myc_ATPS assay using WT IMV

^b Ratio of IC₅₀ in NADH driven Myc_ATPS assay using Δcyt-bc₁/WT IMV

^c Inhibition of O₂ consumption assay using Δcyt-bd membrane

^d Inhibition of O₂ consumption assay using Δcyt-bc₁ membrane

Inhibition of oxygen consumption was observed immediately after compound (**13a**) addition in the oxygen consumption assay which used Δcyt-bd membrane possessing only the cytochrome C oxidase (**Figure 8, right panel**) and not the Δcyt-bc₁ membrane (**Figure 8, left panel**). Rescuing the rate of oxygen consumption by the addition of ascorbate / TMPD despite the presence of the compound in the assay mix having Δcyt-bd membrane (**Figure 8, right panel**) further confirmed the observation. Results from these biochemical tests hinted at cytochrome c oxidase as the target of IPE class of compounds. The reference compound bedaquiline did not inhibit the oxygen consumption assay as expected (data not shown).



Membr: Membrane (IMV)

Figure 8: Oxygen consumption assay. Assay was set up with either $\Delta\text{cyt-bc}_1$ (left panel) or $\Delta\text{cyt-bd}$ (right panel) membrane and the reaction initiated by the addition of NADH. O_2 consumption was monitored over a period of 800 seconds. Compound **13a** was added to the reaction mix between 250-450 seconds. Rescue of the inhibition of O_2 consumption was tested by adding Asc/TMPD.

Despite the potent MIC against *M. tuberculosis* strain, the lack of MIC against *M. smegmatis* wild-type strain in a cell based assay for the IPEs was a bit puzzling. The results obtained in the biochemical deconvolution scheme provided an explanation for this discrepancy. In the wild-type strain, cytochrome bd oxidase which is partially expressed under aerobic conditions most likely compensated the inhibition of cytochrome c oxidase activity when IPEs were present. To confirm this, the compounds were tested against *M. smegmatis* strains lacking either $\Delta\text{cyt-bc}_1$ or $\Delta\text{cyt-aa}_3$ or $\Delta\text{cyt-bd}$ with wild-type *M. smegmatis* strain serving as control. At least a 4-fold down shift in MIC observed with the $\Delta\text{cyt-bd}$ strain as compared to the MICs against either wild-type or $\Delta\text{cyt-bc}_1$ or $\Delta\text{cyt-aa}_3$ strains indicated that the test compounds inhibited the growth of the strain

possessing only cytochrome c oxidase (cytochrome bc₁-aa₃ super complex) (**Table S5**). Thus a series of biochemical tests and cell based assays performed using a number of mutants of the mycobacterial Ox-Phos pathway components provided clear evidence to conclude that cytochrome c oxidase (cytochrome bc₁-aa₃ super complex) is the target of IPE compounds. However, this data could not differentiate whether the molecular target is cytochrome bc₁ oxidase or cytochrome aa₃ oxidase. Since, all known inhibitors of cytochrome aa₃ oxidase are very small molecules like NO, CO, azide, etc., it is highly likely that IPEs inhibit cytochrome bc₁ oxidase similar to the inhibition observed with Q203.³³ As expected, bedaquiline, an inhibitor of ATP synthase, did not show any change in MIC in any of these assays.

IPE, SQA are active against *M. tuberculosis* clinical strains

New drugs needed for the treatment of tuberculosis should have a novel mechanism of action to overcome cross resistance issues with the pre-existing mutant strains in the clinic. A small panel of *M. tuberculosis* clinical strains including a few drug-sensitive and a few single drug-resistant (SDR) strains were tested for MIC with compounds from SQA and IPE series. Bedaquiline mutants generated and characterized in-house were also included in the panel. The data was also expected to indicate the effectiveness of the lead compound against clinical isolates. The 14-day turbidometric MIC measurements for all compounds were the same irrespective of the strain tested, sensitive or SDR. MICs were in the same range as against the wild-type laboratory strain of *M. tuberculosis* (**Table S6**). Similar observation was made with bedaquiline resistant *M. tuberculosis* mutants (**Table S6**) suggesting 1. a mechanism different from the known anti-tubercular drugs used in the panel as well as bedaquiline, 2. potential of SQA compounds to be used in combination with other drugs upon further development. It is not surprising to see that

the bedaquiline mutants used here didn't cross react with SQA compounds as the mutations in the bedaquiline resistant strains were at Ile66 and Ala63.

Pharmacokinetic and pharmacodynamic profiling

A significant improvement in the potency, cytotoxicity and selectivity observed during SAR optimization for these two class of compounds encouraged us to evaluate the oral exposure for the most potent compound from the two series. Due to the high *in vitro* metabolic clearance observed, oral exposure was determined in mouse in the presence of aminobenzotriazole (ABT), a pan CYP inhibitor. Although **19e** (IPE) showed good oral exposure in the presence of ABT at 100 mg/kg, the free levels obtained were not maintained above MIC for adequate duration of time (**Figure 9A**) to test proof of principle in a TB infection model. However, the SQA compound **31f** showed a 300-fold increase in free plasma concentration when administered along with 100 mg/kg ABT (**Figure 9B**). This concentration remained above MIC for over 15 hours and was considered sufficient to go for pharmacodynamic profiling in an acute model of tuberculosis infection.

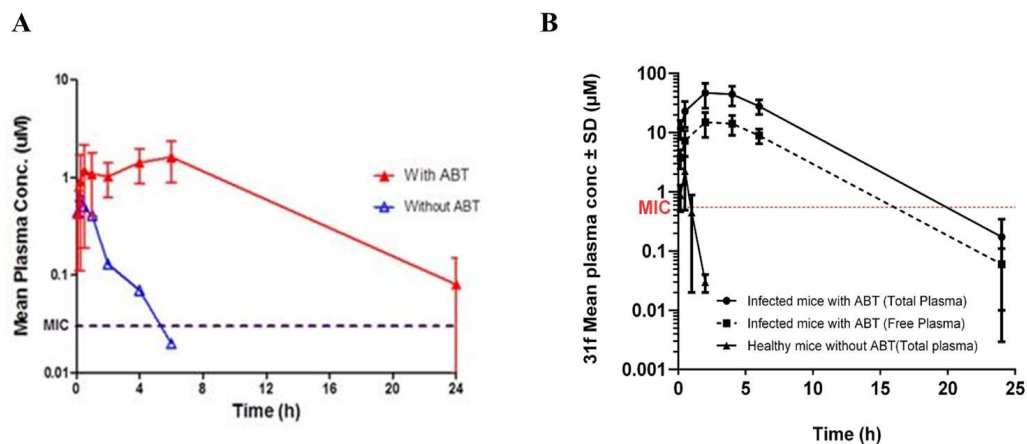


Figure 9. Oral pharmacokinetic profiles of 19e (A), 31f (B). Mouse pharmacokinetic profiles of **19e** and **31f** were generated by administering each compound at 100 mg/kg in the presence of 100 mg/kg ABT.

A two week treatment in a mouse model of acute TB infection was chosen as a test for establishing proof of principle. In this model, the infected mice would be treated with test and reference compounds for two weeks starting from day 3 post-infection and the CFU monitored. A significant increase in the bacterial burden in the lungs of infected but untreated mice as against those which are treated would allow a clear identification of either a static or cidal effect imparted by the test compound.

Mice infected with *M. tuberculosis* were treated with 100 and 200 mg/kg of **31f** for two weeks. Although there was a significant growth inhibition at 100 mg/kg dose, a clear static effect was observed after treatment of infected mice with 200 mg/kg (**Figure 10**), thus establishing the potential of this compound to treat tuberculosis infection in mice.

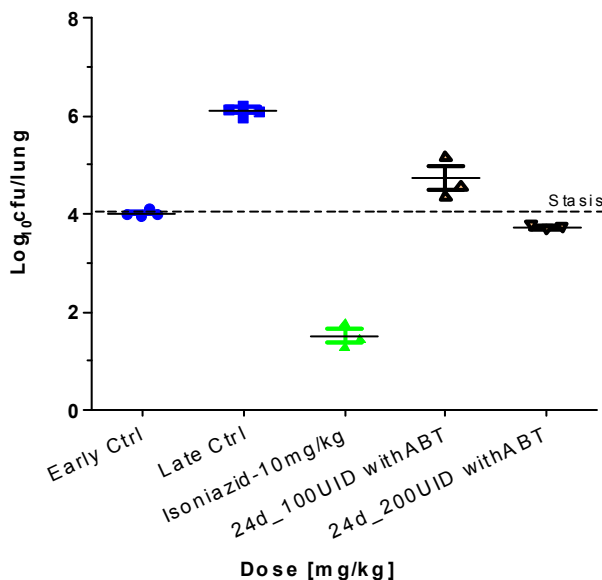


Figure 10: *In vivo* efficacy in a mouse model of acute TB infection. Early control (blue circles), late control (blue squares), isoniazid at 10 mg/kg (green triangles), 31f at 100 mg/kg (black triangles) and 200 mg/kg (black inverted triangles). Dotted line indicates line of stasis which is equivalent to the early control CFU.

SUMMARY AND CONCLUSION

Bedaquiline's discovery from a phenotypic screen and its approval to treat MDR-TB cases validated ATP synthase and the entire Ox-Phos pathway as suitable targets for anti-TB drug discovery. We have demonstrated the use of a pathway screen to identify inhibitors of ATP synthesis pathway as against a single target based biochemical or whole cell based phenotypic screening. The use of secondary selectivity assays and hit triaging efforts resulted in the identification of chemically distinct scaffolds as specific Ox-Phos (ATP synthesis) pathway inhibitors. Further medicinal chemistry efforts on the prioritized chemotypes resulted in building structure activity relationship for potency, selectivity and identification of compounds for *in vivo*

proof of principle. The data generated from a number of specificity and selectivity assays along with potency in the Myc_ATPS assay were used during the design of new molecules and SAR expansion. Although the initial hit rate was very high from the high through put screening of 900,000 compounds, the scheme of assays and tests enabled prioritization of three scaffolds for SAR exploration resulting in the identification of two lead series. Although this is not a typical single target enzyme screen, the output of this HTS was found to be similar in lines with observations made earlier about the low success rates of HTS in anti-bacterial discovery and development programs.⁴⁹

IPE series of molecules were very promising because of their novelty, high potency and selectivity. A novel biochemical deconvolution scheme employed in this study enabled identifying cytochrome c oxidase as its target. However, the bacteriostatic nature (Minimum Bactericidal Concentration (MBC) of a number of IPEs tested were >100 μ M against *M. tuberculosis*, **Table S3**) of compounds from this series combined with poor solubility and poor pharmacokinetic profile resulted in deprioritizing the series for proof of principle testing.

The other lead series, 'squaramide' was found to be very specific and selective without any identified cytotoxicity issues. It retained MIC against a small panel of drug sensitive and single drug resistant strains of *M. tuberculosis* including bedaquiline resistant mutants. Squaramide compound **31f**, although similar to bedaquiline in its mode of action with the resistance mutation mapping to Asp28 of subunit-*c*, mapping of a second mutation to subunit-*a* suggested additional interactions of the compound at the binding site. Unlike in case of bedaquiline, no mutations could be mapped to Ile66 or Ala63 positions. The docking results of the squaramide inhibitors at the active site of the *M. tuberculosis* ATP synthase homology model also supported this hypothesis and could explain the SAR for the series. The compound's potential to arrest the

growth of *M. tuberculosis* in the mouse lungs was demonstrated in an acute TB infection model. A complete stasis observed at the end of a two week treatment with a 200 mg/kg dose established proof of principle. Further medicinal chemistry optimization of the squaramides series towards improving pharmacokinetic properties and *in vivo* safety evaluation are needed to identify a clinical candidate from this series for the treatment of tuberculosis.

EXPERIMENTAL SECTION

Key materials: Mycobacterial inverted membrane vesicles from *M smegmatis* were prepared in-house. Sub mitochondrial particles (SMP) was preparation from Prof. Harvey Rubin's laboratory, University of Pennsylvania. Beetle Luciferin, potassium salt (CAS: E1605) and Quantilum recombinant luciferase (CAS: E1702) were procured from Promega. ATP Bioluminescence kit CLSII (CAS: 11699695001) was purchased from Roche. Lysosensor Green DND-153 (CAS: L7354) was purchased from Life technologies. NADH (CAS: N8129) and ADP (CAS: A2754) were purchased from SIGMA. 384 well black flat bottom plates were procured from Corning (CAS: 3573). Reference inhibitors: Dicyclohexylcarbodiimide (DCCD, Catalog no: D80002), Thioridazine (CAS: T-9025) and carbonylchloride 3-chlorophenyl hydrazone (CCCP, CAS: C2759) were procured from SIGMA. Bedaquiline was synthesized in house.

NADH driven ATP synthesis assay (Myc_ATPS):

The ATP synthesis activity was determined in isolated membrane vesicles from *M. smegmatis* that were prepared according to Yano *et al.*⁴¹ The 384 well plate assay with an assay volume of 30 μ l used 8 μ g/ml *M. smegmatis* inverted membrane vesicles (IMVs). Briefly, 15 μ l of enzyme mix containing IMVs and 5 mM MgCl₂ in HEPES-NaOH buffer, pH 7.6 was added to 384 well plates containing 1 μ l of 30X compound dilutions. The reaction was initiated by adding 15 μ l of

substrate mix containing 0.3 mM NADH, 15 μ M ADP and 0.1 mM KH_2PO_4 . Plates were incubated for 60 min at room temperature. The amount of ATP synthesized is measured by adding 30 μ l of Luciferin/luciferase reagent and the luminescence measured using TECAN Infinite F500 immediately. IC_{50} values were calculated using GraphPad Prism software.

Mitochondrial ATP synthesis assay (SMP_ATPS):

The ATP synthesized by mitochondrial ATP synthase using ADP and inorganic phosphate, Pi was measured using ATP Bioluminescence Assay Kit CLS II and purified bovine SMP. Briefly, 20 μ l of reagent mix-1 (purified bovine SMP along with ADP, potassium phosphate and CLSII detection reagent in Tris acetate buffer, pH 7.5) was added to 384 well black plates containing 30X compound dilutions. Reaction was initiated by the addition of 10 μ l of reagent mix-2 containing 0.2 mM NADH. Luminescence was read kinetically in Tecan Infinite F500 up to 20 minutes. IC_{50} values were calculated using GraphPad Prism software.

Membrane damage assay in BCG:

M. bovis BCG cells were grown in 7H9 media containing 10% ADC. At A_{600} 0.5-0.6, cells were harvested and resuspended in 7H9 media such that the A_{600} is about 3.0. Cells were then loaded with the fluorescence probe, DiOC₂ at a final concentration of 1 μ M and incubated for 30 minutes in dark. After 30 minutes, 10 μ l of cell suspension ($\sim 10^7$ cells) was dispensed onto 384 well plates containing 1 μ l of 30X compound dilutions and 39 μ l 7H9 media bringing the total assay volume to 50 μ l using multidrop. Plates were incubated in the dark for 60 minutes and fluorescence was read in Tecan Safire with excitation at 485 nm and emission at 600 nm. DiOC₂ has delocalized positive charge and can penetrate the bacterial membrane and accumulate on the inner negative surface. Stacked DiOC₂ molecules have an excitation maxima at 488 nm and emission at 600 nm. Fluorescence is higher with high membrane potential. CCCP, a proton

ionophore is used as positive control for membrane damage. IC₅₀ values were calculated using GraphPad Prism software.

Δ pH assay to identify disruptors of the proton gradient:

Δ pH assay performed with mycobacterial membrane vesicles utilized a pH sensitive probe, Lysosensor Green DND 153. The assay components were identical to the primary ATP synthesis assay without the substrates of ATP synthase ADP and Pi whose addition would otherwise take reaction to completion and dissipate ΔpH. Fluorescence is quenched when NADH is present, due to the formation of ΔpH. Fluorescence quenching is inhibited by thioridazine and is used as positive control for the assay. Briefly, 15 μl of substrate mix containing 0.3 mM NADH and 100 nM Lysosensor green DND-153 was added to 384 well plates containing 1 μl of 30X compound dilutions. The reaction was initiated by adding 15 μl of membrane mix containing 8 μg/ml *M. smegmatis* membrane vesicles and 5 mM MgCl₂ in HEPES-NaOH buffer, pH 7.6. Plates were incubated for 30 min at room temperature. Fluorescence was measured in Tecan Infinite F500 using excitation at 485 nm and emission at 520nm. IC₅₀ values were calculated using GraphPad Prism software.

Microbiology methods:

Determination of minimum inhibitory concentration (MIC), minimum bactericidal concentration (MBC) were performed as reported earlier.⁵⁰ For an initial MIC₉₀ estimate, a small set of *M. tuberculosis* clinical strains which included a set of sensitive strains and a set of single drug resistant strains were used to test the MIC. Concentration of the compound at which ≥ 80% growth inhibition in a turbidometric read method was considered as MIC. In-house generated bedaquiline^R strains having I66M and A63P mutations were also used to test cross resistance with the compounds.

Mammalian MIC (cytotoxicity):

IC₅₀ for compounds were determined in an assay which used either A549 or THP1 cell lines. The assays were performed as described previously⁵¹ with A549 cell line. Briefly, A549 cells were exposed to different concentrations of compounds in a 384 well plate assay for 72 hours at 37 °C with 5% CO₂. The proliferation / inhibition of proliferation was measured using the redox indicator alamar blue.

The assay with THP1 cells is performed in similar lines with A549 assay except that the incubation time with compounds is reduced to 24 hours in a 96 well plate with 100 µl assay volume. About 4X10⁴ cells / well in 95 µl of media were exposed to 5 µl of compound (20X concentrated). After 24 hours of incubation, 20 µl of rezasurin was added and fluorescence read at 560/590 nm following a 2 hour incubation at 37 °C.

These cell lines were procured from ATCC and periodically tested for functionality and mycoplasma contamination.

Mutation mapping:

Whole genome sequencing to identify **31f** mutants were performed as described in Shirude *et al.*⁵¹

Pharmacokinetic and pharmacodynamic studies in mice:

The animal studies were approved by the Institutional Animal Ethics Committee (IAEC). Oral exposure determination of **19e** was carried out in healthy BALB/c mice. This compound was suspended in 0.5% hydroxypropyl methyl cellulose (HPMC) & Tween80, and was administered at a dose volume of 10 mL/kg to achieve a dose of 100 mg/kg. Blood samples were collected from groups of 3 mice per time point by puncturing the saphenous vein at 5 min, 15 min, 30 min, 1 h, 2 h, 4 h, 6 h, or 8 h and 24 h after dosing. Aminobenzotriazole (ABT) at a dose of 100 mg/kg

was administered orally 2 hours before the test compound administration. Plasma was separated from blood samples by centrifuging at a speed of 10000 rpm at 4 °C and stored at -80 °C until LC-MS/MS analysis. Plasma samples were precipitated with ice cold 90% (v/v) acetonitrile, the samples were analyzed by liquid chromatography-tandem mass spectrometry (LC-MS/MS). Pharmacokinetic analysis was performed with time vs. plasma concentration data by using Phoenix WinNonlin 6.2 software. Following PK parameters, C_{max}, T_{max}, AUC (Area under the plasma concentration), t_{1/2} were estimated using non-compartmental analysis.

Pharmacokinetics of **31f** was analyzed in healthy as well as infected mice during the efficacy study. Blood samples from infected animals were collected and processed in a biosafety level 3 (BSL3) laboratory. **31f** was orally administered in a suspension containing 0.5% hydroxypropyl methylcellulose (HPMC) & Tween 80 at a 10 mL/kg dose volume. Blood samples were collected from groups of 3 mice per time point by puncturing the saphenous vein at 5 min, 15 min, 30 min, 1 h, 2 h, 4 h, 6 h, or 8 h and 24 h after dosing. After precipitation of plasma proteins with 90% (vol/vol) acetonitrile, the samples were analyzed by liquid chromatography-tandem mass spectrometry (LC-MS/MS). Area under the concentration versus time PK profile (AUC) was calculated by non-compartmental analysis (WinNonLin 5.2.1; Pharsight Inc.).

Pharmacodynamics:

BALB/c mice were infected in an aerosol chamber (10⁴ CFU of *M. tuberculosis* H37Rv per mouse) in the acute model. Infected mice were housed in individually ventilated cages (Allentown Technologies, USA) in a BSL3 facility. Treatment was initiated after 3 days of infection. Vehicle and compound treated groups contained 3 mice each. An additional 3 mice were sacrificed just after infection to serve as early controls. **31f** and isoniazid were formulated in 0.5% HPMC/Tween. Infected mice were treated with an oral dose of 100 or 200 mg/kg of **31f**

or 10 mg/kg of isoniazid, once daily, 6 days per week, for 2 weeks. ABT, a known cytochrome P450 inhibitor, was dissolved in water and orally administered at a dose of 100 mg/kg (10 mL/kg), 2 h before dosing the compound to reduce the first pass metabolism and increase plasma exposure. Mice were sacrificed after completion of treatment, and suitable dilutions of their lung homogenates were plated on 7H11 agar to determine viable CFU in mouse lung tissue. One-way analysis of variance (ANOVA) followed by the Bonferroni's multiple-comparison test was used for analyzing efficacy data.

General chemistry methods. All commercial reagents and solvents were used without further purification. Analytical thin-layer chromatography (TLC) was performed on SiO₂ plates on alumina. Visualization was accomplished by UV irradiation at 254 and 220 nm. Flash column chromatography was performed using the Biotage Isolera flash purification system with SiO₂ 60 (particle size 0.040–0.055 mm, 230–400 mesh). Purity of all final derivatives for biological testing was confirmed to be >95% as determined using the following conditions: a Shimadzu HPLC instrument with a Hamilton reverse phase column (HxSil, C18, 3 μm, 2.1 mm × 50 mm (H₂)). Eluent A: 5% CH₃CN in H₂O, eluent B: 90% CH₃CN in H₂O. A flow rate of 0.2 mL/min was used with UV detection at 254 and 214 nm. The structure of the intermediates and end products was confirmed by ¹H NMR and mass spectroscopy. Proton magnetic resonance spectra were determined in DMSO- *d*₆ unless otherwise stated, using Bruker DRX-300 or Bruker DRX-400 spectrometers, operating at 300 MHz or 400 MHz, respectively. Splitting patterns are indicated as follows: s, singlet; d, doublet; t, triplet; m, multiplet; br, broad peak. LCMS data was acquired using Agilent LCMS VL series. Source: ES ionization, coupled with an Agilent 1100 series HPLC system and an Agilent 1100 series PDA as the front end. HRMS data was acquired

using an Agilent 6520, Quadrupole-Time of flight tandem mass spectrometer (Q-ToF MS/MS) coupled with an Agilent 1200 series HPLC system. All anhydrous solvents, reagent grade solvents for chromatography and starting materials were purchased from either Sigma Aldrich Chemical Co. or Fisher Scientific. Water was distilled and purified through a Milli-Q water system (Millipore Corp., Bedford, MA). General methods of purification of compounds involved the use of preloaded silica cartridges purchased from Grace purification systems and/or recrystallization. The reactions were monitored by TLC on pre-coated Merck 60 F₂₅₄ silica gel plates and visualized using UV light (254 nm).

General procedures for Imidazolopyridine ether

2-Phenylimidazo[1,2-a]pyridin-3-ol (3a).

To a solution of 2-aminopyridine (1.861 g, 19.77 mmol) in toluene (45 mL), 2-oxo-2-phenylacetaldehyde (2.65 g, 19.77 mmol) was added portion wise and the reaction mixture was stirred overnight at RT. The reaction mixture was concentrated under reduced pressure to give 2-phenylimidazo[1,2-a]pyridin-3-ol (4.02 g, 97.0%) as a yellowish amorphous powder. m/z (ES⁺), [M+H]⁺ = 211; ¹H NMR (300 MHz, DMSO-*d*₆) δ ppm 6.54 (br. s., 1H) 6.96 - 7.09 (m, 2H) 7.29 - 7.46 (m, 5H) 7.46 - 7.68 (m, 1H) 8.00 (d, J = 7.91 Hz, 3H) 8.25 (d, J = 6.59 Hz, 1H) 12.83 (br. s., 1H).

6-Chloro-2-phenylimidazo[1,2-a]pyridin-3-ol (3b).

To a solution of 5-chloropyridin-2-amine (2.54 g, 19.77 mmol) in dichloromethane (100 mL), 2-oxo-2-phenylacetaldehyde (2.65 g, 19.77 mmol) was added portion wise followed by $\text{BF}_3 \cdot \text{OEt}_2$ (0.025 mL, 0.20 mmol) and the reaction mixture stirred overnight at RT. The suspension filtered and the solid was washed with DCM (10 mL) followed by drying under vacuum to give 6-chloro-2-phenylimidazo[1,2-a]pyridin-3-ol (1.130 g, 23.4%) as a yellowish amorphous powder. m/z (ES^+), $[\text{M}+\text{H}]^+ = 245$; ^1H NMR (300 MHz, $\text{DMSO}-d_6$) δ ppm 7.10 (d, $J = 7.16$ Hz, 1H) 7.30 - 7.49 (m, 4H) 8.01 (d, $J = 7.72$ Hz, 2H) 8.33 (s, 1H) 13.18 (br. s., 1H).

3-Hydroxy-2-phenylimidazo[1,2-a]pyridine-6-carbonitrile (3c).

To a solution of 6-aminonicotinonitrile (2.355 g, 19.77 mmol) in dichloromethane (100 mL), 2-oxo-2-phenylacetaldehyde (2.65 g, 19.77 mmol) was added portion wise followed by $\text{BF}_3 \cdot \text{OEt}_2$ (0.025 mL, 0.20 mmol) and the reaction mixture was stirred overnight at RT. The suspension filtered and the solid was washed with DCM (10 mL) followed by drying under vacuum to give 3-hydroxy-2-phenylimidazo[1,2-a]pyridine-6-carbonitrile (3.30 g, 71.0%) as a yellowish amorphous powder. m/z (ES^+), $[\text{M}+\text{H}]^+ = 236$.

6-Methyl-2-phenylimidazo[1,2-a]pyridin-3-ol (3d).

To a solution of 5-(trifluoromethyl)pyridin-2-amine (3.529 g, 21.77 mmol) in dichloromethane (100 mL), 2-oxo-2-phenylacetaldehyde (2.92 g, 21.77 mmol) was added portion wise and the reaction mixture stirred overnight at RT. The suspension filtered and the solid was washed with DCM (10 mL) followed by drying under vacuum to give 2-phenyl-6-(trifluoromethyl)imidazo[1,2-a]pyridin-3-ol (5.20 g, 86.0%) as a yellowish amorphous powder. m/z (ES^+), $[\text{M}+\text{H}]^+ = 225$; ^1H NMR (300 MHz, $\text{DMSO}-d_6$) δ ppm 6.48 - 6.62 (m, 1H) 6.67 - 6.80

(m, 2H) 6.85 (d, $J = 8.85$ Hz, 1H) 7.47 - 7.59 (m, 2H) 7.65 (q, $J = 6.91$ Hz, 1H) 7.77 (d, $J = 8.67$ Hz, 1H) 7.99 - 8.15 (m, 3H) 8.39 (s, 1H).

2-(4-Fluorophenyl)-6-methylimidazo[1,2-a]pyridin-3-ol (3e).

To a solution of 5-methylpyridin-2-amine (1.0 g, 9.25 mmol) in DCM (41 mL), 2-(4-fluorophenyl)-2-oxoacetaldehyde (1.407 g, 9.25 mmol) was added portion wise and the reaction mixture stirred overnight at RT. The reaction mixture was concentrated under reduced pressure to give 2-(4-fluorophenyl)-6-ethylimidazo[1,2-a]pyridin-3-ol (1.620 g, 72.3%) as a yellowish amorphous powder. m/z (ES^+), $[M+H]^+ = 243$; 1H NMR (300 MHz, DMSO- d_6) δ ppm 2.32 (s, 3H) 7.15 - 7.27 (m, 3H) 7.32 - 7.38 (m, 1H) 7.98 - 8.06 (m, 2H) 8.09 (br. s., 1H) 12.72 (br. s., 1H).

3-(3-Phenoxypropoxy)-2-phenylimidazo[1,2-a]pyridine (4a).

To a solution of 2-phenylimidazo[1,2-a]pyridin-3-ol (0.718 g, 3.42 mmol) in DMF (11 mL), sodium hydride (0.150 g, 3.76 mmol) was added at 0 °C. After stirring for 10 min, (3-bromopropoxy)benzene (0.808 g, 3.76 mmol) was added and the reaction mixture stirred at RT for 3 h. The reaction mixture was poured onto ice-water (30 mL) and extracted with EtOAc (30 mL x 3). The combined organic layer was washed with brine and water (30 mL x 3) and dried over Na_2SO_4 . The organic layer was concentrated to give a residue which was purified by reverse phase HPLC to give 3-(3-Phenoxypropoxy)-2-phenylimidazo[1,2-a]pyridine (0.114, 9.7%) as a liquid. HRMS m/z ($M + H^+$) calcd for $[C_{22}H_{20}N_2O_2 + H]^+$ 345.15975, found 345.1593; 1H NMR (300 MHz, DMSO- d_6) δ ppm 2.31 (t, $J = 5.84$ Hz, 2H) 4.26 (t, $J = 5.75$ Hz, 4H) 6.89 (t, $J = 6.69$

Hz, 1H) 6.93 - 7.04 (m, 3H) 7.17 - 7.38 (m, 6H) 7.52 (d, $J = 9.04$ Hz, 1H) 8.00 (d, $J = 7.35$ Hz, 2H) 8.25 (d, $J = 6.78$ Hz, 1H).

6-Chloro-3-(3-phenoxypropoxy)-2-phenylimidazo[1,2-a]pyridine (4b).

To a solution of 6-chloro-2-phenylimidazo[1,2-a]pyridin-3-ol (0.273 g, 1.12 mmol) and (3-bromopropoxy)benzene (0.288 g, 1.34 mmol) in DMF (6 mL), sodium hydride (0.054 g, 1.34 mmol) was added at 0 °C and the reaction mixture stirred at RT for 12 h. The reaction mixture was poured onto ice-water (20 mL) and extracted with EtOAc (20 mL x 3). The combined organic layer was washed with brine and water (20 mL x 3) and dried over Na₂SO₄. The organic layer was concentrated to give residue which was purified by reverse phase HPLC to give 6-chloro-3-(3-phenoxypropoxy)-2-phenylimidazo[1,2-a]pyridine (0.085 g, 20.11 %) as an amorphous powder. HRMS m/z (M + H)⁺ calculated for [C₂₂H₁₉ClN₂O₂ + H]⁺ 379.12075, found 379.1214; ¹H NMR (300 MHz, DMSO-*d*₆) δ ppm 2.24 - 2.39 (m, 2H) 4.26 (q, $J = 5.65$ Hz, 4H) 6.93 - 7.04 (m, 3H) 7.21 - 7.38 (m, 6H) 7.57 (d, $J = 9.61$ Hz, 1H) 7.98 (d, $J = 7.35$ Hz, 2H) 8.49 (s, 1H).

3-(3-Phenoxypropoxy)-2-phenylimidazo[1,2-a]pyridine-6-carbonitrile (4c).

To a solution of 3-hydroxy-2-phenylimidazo[1,2-a]pyridine-6-carbonitrile (0.508 g, 2.16 mmol) in DMF (10 mL), sodium hydride (0.104 g, 2.59 mmol) was added at 0 °C. After 10 min, (3-bromopropoxy)benzene (0.511 g, 2.38 mmol) was added and the reaction mixture stirred at RT for 12 h. The reaction mixture was poured onto ice-water (30 mL) and extracted with EtOAc (30 mL x 3). The combined organic layer was washed with brine and water (30 mL x 3) and dried

over Na₂SO₄. The organic layer was concentrated to give residue which was purified by reverse phase HPLC to give 3-(3-Phenoxypropoxy)-2-phenylimidazo[1,2-a]pyridine-6-carbonitrile (0.010 g, 1.2%) as an amorphous powder. HRMS m/z (M + H)⁺ calculated for [C₂₃H₁₉N₃O₂ + H]⁺ 370.15495, found 370.1555; ¹H NMR (300 MHz, DMSO-d₆) δ ppm 2.31 - 2.38 (m, 2 H) 4.28 (dt, J = 17.66, 5.96 Hz, 4 H) 6.99 (d, J = 8.48 Hz, 3 H) 7.22 - 7.37 (m, 5 H) 7.46 (d, J = 8.67 Hz, 1 H) 7.68 (d, J = 9.04 Hz, 1 H) 7.99 (br. s., 2 H) 9.17 (s, 1 H).

6-Methyl-3-(3-phenoxypropoxy)-2-phenylimidazo[1,2-a]pyridine (4d).

To a solution of 6-methyl-2-phenylimidazo[1,2-a]pyridin-3-ol (0.440 g, 1.96 mmol) and (3-bromopropoxy)benzene (0.506 g, 2.35 mmol) in DMF (10 mL), sodium hydride (0.094 g, 2.35 mmol) was added at 0 °C and the reaction mixture stirred for at RT 12 h. The reaction mixture was poured onto ice-water (20 mL) and extracted with EtOAc (20 mL x 3). The combined organic layer was washed with brine and water (20 mL x 3) and dried over Na₂SO₄. The organic layer was concentrated to give residue which was purified by reverse phase HPLC to give 6-methyl-3-(3-phenoxypropoxy)-2-phenylimidazo[1,2-a]pyridine (0.281 g, 40%) as a white amorphous powder. HRMS m/z (M + H)⁺ calculated for [C₂₃H₂₂N₂O₂ + H]⁺ 359.17535, found 359.1760; ¹H NMR (300 MHz, DMSO-d₆) δ ppm 2.20 (s, 3 H) 2.32 (quin, J = 5.93 Hz, 2 H) 4.17 - 4.33 (m, 4 H) 6.93 - 7.09 (m, 4 H) 7.19 - 7.38 (m, 5 H) 7.42 (d, J = 9.23 Hz, 1 H) 7.94 - 8.03 (m, 3 H).

3-(2-(4-Fluorophenoxy)ethoxy)-2-phenylimidazo[1,2-a]pyridine (5a).

To a solution of 2-phenylimidazo[1,2-a]pyridin-3-ol (0.481 g, 2.29 mmol) and 1-(2-bromoethoxy)-4-fluorobenzene (0.601 g, 2.75 mmol) in DMF (12 mL), sodium hydride (0.110 g,

2.75 mmol) was added at 0 °C and the reaction mixture stirred at RT for 12 h . The reaction mixture was poured onto ice-water (20 mL) and extracted with EtOAc (20 mL x 3). The combined organic layer was washed with brine and water (20 mL x 3) and dried over Na₂SO₄. The organic layer was concentrated to give residue which was purified by reverse phase HPLC to give 3-(2-(4-fluorophenoxy)ethoxy)-2-phenylimidazo[1,2-a]pyridine (0.181 g, 22.7%) as a liquid. HRMS m/z (M + H)⁺ calculated for [C₂₁H₁₇FN₂O₂ + H]⁺ 349.13465, found 349.1349; ¹H NMR (300 MHz, DMSO-*d*₆) δ ppm 4.34 (br. s., 2 H) 4.43 (br. s., 2 H) 6.88 - 7.04 (m, 3 H) 7.09 - 7.34 (m, 4 H) 7.37 - 7.47 (m, 2 H) 7.53 (d, *J* = 9.04 Hz, 1 H) 8.10 (d, *J* = 7.72 Hz, 2 H) 8.32 (d, *J* = 6.78 Hz, 1 H).

6-Chloro-3-(2-(4-fluorophenoxy)ethoxy)-2-phenylimidazo[1,2-a]pyridine (5b).

To a solution of 6-chloro-2-phenylimidazo[1,2-a]pyridin-3-ol (0.36 g, 1.47 mmol) and 1-(2-bromoethoxy)-4-fluorobenzene (0.387 g, 1.77 mmol) in DMF (12 mL), sodium hydride (0.071 g, 1.77 mmol) was added at 0 °C and the reaction mixture stirred for at RT 12 h. The reaction mixture was poured onto ice-water (20 mL) and extracted with EtOAc (20 mL x 3). The combined organic layer was washed with brine and water (20 mL x 3) and dried over Na₂SO₄. The organic layer was concentrated to give a residue which was purified by reverse phase HPLC to give the title compound (0.245 g, 43.5%) as an amorphous powder. HRMS m/z (M + H)⁺ calculated for [C₂₁H₁₆ClFN₂O₂ + H]⁺ 383.09565, found 383.0961; ¹H NMR (300 MHz, DMSO-*d*₆) δ ppm 4.36 (br. s., 2 H) 4.46 (br. s., 2 H) 6.97 (dd, *J* = 8.38, 4.24 Hz, 2 H) 7.16 (t, *J* = 8.48 Hz, 2 H) 7.22 - 7.36 (m, 2H) 7.38 - 7.49 (m, 2 H) 7.58 (d, *J* = 9.61 Hz, 1 H) 8.08 (d, *J* = 7.72 Hz, 2 H) 8.53 (s, 1 H).

3-(2-(4-Fluorophenoxy)ethoxy)-6-methyl-2-phenylimidazo[1,2-a]pyridine (5d).

To a solution of 6-methyl-2-phenylimidazo[1,2-a]pyridin-3-ol (0.440 g, 1.96 mmol) and 1-(2-bromoethoxy)-4-fluorobenzene (0.516 g, 2.35 mmol) in DMF (10 mL), sodium hydride (0.094 g, 2.35 mmol) was added at 0 °C and the reaction mixture stirred for at RT 12 h. The reaction mixture was poured onto ice-water (20 mL) and extracted with EtOAc (20 mL x 3). The combined organic layer was washed with brine and water (20 mL x 3) and dried over Na₂SO₄. The organic layer was concentrated to give residue which was purified by reverse phase HPLC to give 3-(2-(4-fluorophenoxy)ethoxy)-6-methyl-2-phenylimidazo[1,2-a]pyridine (0.225 g, 31.6%) as a white amorphous powder. HRMS m/z ($M + H$)⁺ calculated for [C₂₂H₁₉FN₂O₂ + H]⁺ 363.15025, found 363.1498; ¹H NMR (300 MHz, DMSO-*d*₆) δ ppm 2.24 (s, 3 H) 4.33 (d, J = 4.14 Hz, 2 H) 4.42 (d, J = 4.14 Hz, 2 H) 6.95 - 7.03 (m, 2 H) 7.04 - 7.10 (m, 1 H) 7.12 - 7.20 (m, 2 H) 7.24 - 7.32 (m, 1 H) 7.37 - 7.46 (m, 3 H) 8.04 - 8.11 (m, 3 H).

3-(2-(4-Fluorophenoxy)ethoxy)-2-(4-fluorophenyl)-6-methylimidazo[1,2-a]pyridine (6e).

To a solution of 2-(4-fluorophenyl)-6-methylimidazo[1,2-a]pyridin-3-ol (0.200 g, 0.83 mmol) and 1-(2-bromoethoxy)-4-fluorobenzene (0.217 g, 0.99 mmol) in DMF (4 mL), sodium hydride (0.040 g, 0.99 mmol) was added at 0 °C and the reaction mixture was stirred for at RT 12 h. The reaction mixture was poured onto ice-water (20 mL) and extracted with EtOAc (20 mL x 3). The combined organic layer was washed with brine and water (20 mL x 3) and dried over Na₂SO₄. The organic layer was concentrated to give residue which was purified by reverse phase HPLC to give 3-(2-(4-fluorophenoxy)ethoxy)-2-(4-fluorophenyl)-6-methylimidazo[1,2-a]pyridine (0.060 g, 19.1%) as a white amorphous powder. HRMS m/z ($M + H$)⁺ calculated for [C₂₂H₁₈F₂N₂O₂ + H]⁺ 381.14085, found 381.1388; ¹H NMR (300 MHz, DMSO-*d*₆) δ ppm 2.25 (s, 3 H) 4.31 (d, J =

3.58 Hz, 2 H) 4.42 (d, $J = 3.77$ Hz, 2 H) 6.98 (dd, $J = 9.14, 4.43$ Hz, 2 H) 7.05 - 7.28 (m, 5 H)
7.43 (d, $J = 9.23$ Hz, 1 H) 8.04 - 8.13 (m, 3 H).

4-(2-(6-Chloro-2-phenylimidazo[1,2-a]pyridin-3-yloxy)ethyl)morpholine (7b).

To a solution of 4-(2-chloroethyl)morpholine hydrochloride (0.380 g, 2.04 mmol) and 6-chloro-2-phenylimidazo[1,2-a]pyridin-3-ol (0.320 g, 1.31 mmol) in DMF (7 mL), sodium hydride (0.126 g, 3.14 mmol) was added at 0 °C. After 20 min, the tetrabutylammonium iodide (0.029 g, 0.08 mmol) was added and the reaction mixture allowed to warm to RT and stirred for 48h. The reaction mixture was poured onto ice-water (20 mL) and extracted with EtOAc (20 mL x 3). The combined organic layer was washed with brine and water (20 mL x 3) and dried over Na₂SO₄. The organic layer was concentrated to give residue which was purified by reverse phase HPLC to give 4-(2-(6-chloro-2-phenylimidazo[1,2-a]pyridin-3-yloxy)ethyl)morpholine (0.028 g, 5.98%) as a brownish amorphous powder. HRMS m/z ($M + H$)⁺ calculated for [C₁₉H₂₀ClN₃O₂ + H]⁺ 358.13165, found 358.1314; ¹H NMR (300 MHz, DMSO-d₆) δ ppm 2.38 (br. s., 4 H) 2.67 (br. s., 2 H) 3.53 (br. s., 4 H) 4.24 (br. s., 2 H) 7.26 (d, $J = 9.61$ Hz, 1 H) 7.29 - 7.38 (m, 1 H) 7.48 (t, $J = 7.44$ Hz, 2 H) 7.56 (d, $J = 9.98$ Hz, 1 H) 8.06 (d, $J = 7.72$ Hz, 2 H) 8.75 (s, 1 H)

3-(3-Methoxypropoxy)-2-phenylimidazo[1,2-a]pyridine (8a).

To a solution of 2-phenylimidazo[1,2-a]pyridin-3-ol (0.52 g, 2.47 mmol) and 3-methoxypropyl methanesulfonate (0.624 g, 3.71 mmol) in DMF (13 mL), sodium hydride (0.119 g, 2.97 mmol) was added at 0 °C and the reaction mixture stirred for at RT 12 h. The reaction mixture was poured onto ice-water (20 mL) and extracted with EtOAc (20 mL x 3). The combined organic

layer was washed with brine and water (20 mL x 3) and dried over Na₂SO₄. The organic layer was concentrated to give residue which was purified by reverse phase HPLC to give 3-(3-methoxypropoxy)-2-phenylimidazo[1,2-a]pyridine (0.190g, 27.2%) as a gum. HRMS *m/z* (M + H)⁺ calculated for [C₁₇H₁₈N₂O₂ + H]⁺ 283.14405, found 283.1454; ¹H NMR (300 MHz, DMSO-*d*₆) δ ppm 2.07 (quin, *J* = 5.98 Hz, 2 H) 3.29 (s, 3 H) 3.57 (t, *J* = 5.93 Hz, 2 H) 4.13 (t, *J* = 6.22 Hz, 2 H) 6.94 (t, *J* = 6.69 Hz, 1 H) 7.22 (t, *J* = 7.82 Hz, 1 H) 7.27 - 7.36 (m, 1 H) 7.42 - 7.57 (m, 3 H) 8.03 (d, *J* = 7.72 Hz, 2 H) 8.24 (d, *J* = 6.78 Hz, 1 H).

2-Phenyl-3-(3-(pyrimidin-5-yloxy)propoxy)imidazo[1,2-a]pyridine (9a).

To a solution of 2-phenylimidazo[1,2-a]pyridin-3-ol (0.385 g, 1.83 mmol) and 5-(3-bromopropoxy)pyrimidine (0.477 g, 2.20 mmol) in DMF (9 mL), sodium hydride (0.088 g, 2.20 mmol) was added at 0 °C and the reaction mixture was stirred for at RT 12 h. The reaction mixture was poured onto ice-water (20 mL) and extracted with EtOAc (20 mL x 3). The combined organic layer was washed with brine and water (20 mL x 3) and dried over Na₂SO₄. The organic layer was concentrated to give residue which was purified by reverse phase HPLC to give 2-phenyl-3-(3-(pyrimidin-5-yloxy)propoxy)imidazo[1,2-a]pyridine (0.245 g, 38.6%) as a gum. HRMS *m/z* (M + H)⁺ calculated for [C₂₀H₁₈N₄O₂ + H]⁺ 347.15025, found 347.1478; ¹H NMR (300 MHz, DMSO-*d*₆) δ ppm 2.35 (t, *J* = 5.84 Hz, 2 H) 4.26 (t, *J* = 5.84 Hz, 2 H) 4.44 (t, *J* = 5.84 Hz, 2 H) 6.92 (t, *J* = 6.59 Hz, 1 H) 7.18 - 7.37 (m, 4 H) 7.52 (d, *J* = 9.04 Hz, 1 H) 7.99 (d, *J* = 7.54 Hz, 2 H) 8.28 (d, *J* = 6.78 Hz, 1 H) 8.61 (s, 2 H) 8.85 (s, 1 H).

3-(6-Methyl-2-phenylimidazo[1,2-a]pyridin-3-yloxy)propan-1-ol (10d).

6-Methyl-2-phenylimidazo[1,2-a]pyridin-3-ol (0.217 g, 0.97 mmol), 3-bromo-1-propanol (0.085 mL, 0.97 mmol) and potassium carbonate (0.669 g, 4.84 mmol) were stirred together in DMF (5 mL) under N₂ for at RT 16 h. The reaction mixture was quenched by adding water (20 mL) and extracted with EtOAc (20 mL x 3). The combined organic layer was washed with brine (20 mL x 3) and dried over Na₂SO₄ and evaporated on a rotavap. The residue was purified by silica gel column chromatography to give 3-(6-methyl-2-phenylimidazo[1,2-a]pyridin-3-yloxy)propan-1-ol (0.161 g, 59.1%) as a gum. ESI *m/z* (ES⁺), [M+H]⁺ = 283; ¹H NMR (300 MHz, DMSO-*d*₆) δ ppm 1.99 (quin, *J* = 6.31 Hz, 2 H) 2.32 (s, 3 H) 3.66 (q, *J* = 5.84 Hz, 2 H) 4.16 (t, *J* = 6.50 Hz, 2 H) 4.68 (t, *J* = 4.99 Hz, 1 H) 7.07 (d, *J* = 9.23 Hz, 1 H) 7.25 - 7.34 (m, 1 H) 7.39 - 7.50 (m, 3 H) 7.98 - 8.10 (m, 3 H).

3-((2-(4-Fluorophenyl)-6-methylimidazo[1,2-a]pyridin-3-yl)oxy)propan-1-ol (11e).

2-(4-Fluorophenyl)-6-methylimidazo[1,2-a]pyridin-3-ol (1.0 g, 4.13 mmol), 3-bromo-1-propanol (0.361 mL, 4.13 mmol) and potassium carbonate (2.85 g, 20.64 mmol) were stirred together in DMF (5 mL) under N₂ at RT for 16 h. The reaction mixture was quenched by adding water (20 mL) and extracted with EtOAc (20 mL x 3). The combined organic layer was washed with brine (20 mL x 3) and dried over Na₂SO₄ and evaporated on a rotavap to give a residue which was purified by column chromatography to give 3-((2-(4-fluorophenyl)-6-methylimidazo[1,2-a]pyridin-3-yl)oxy)propan-1-ol (0.777 g, 62.7%) as an amorphous powder. HRMS *m/z* (M + H)⁺ calculated for [C₁₇H₁₇FN₂O₂ + H]⁺ 301.13465, found 301.1332; ¹H NMR (300 MHz, DMSO-*d*₆) δ ppm 1.98 (quin, *J* = 6.31 Hz, 2 H) 2.32 (s, 3 H) 3.61 - 3.70 (m, 2 H) 4.15 (t, *J* = 6.40 Hz, 2 H) 4.68 (br. s., 1 H) 7.10 (d, *J* = 9.23 Hz, 1 H) 7.29 (t, *J* = 8.95 Hz, 2 H) 7.43 (d, *J* = 9.04 Hz, 1 H) 7.99 - 8.11 (m, 3 H).

3-(6-Methyl-2-phenylimidazo[1,2-a]pyridin-3-yloxy)propyl methanesulfonate (12d).

Methanesulfonyl chloride (0.051 mL, 0.66 mmol) was added to a solution of 3-((6-methyl-2-phenylimidazo[1,2-a]pyridin-3-yl)oxy)propan-1-ol (0.155 g, 0.55 mmol) and triethylamine (0.230 mL, 1.65 mmol) in CH₂Cl₂ (5 mL) at 0 °C. The reaction mixture was allowed to warm to RT and stirred for 3 h. The reaction mixture was transferred to a separatory funnel and washed with saturated NaHCO₃ (20 mL). The organic layer was evaporated on a rotavap to give a brown oil which was used as such for the next step without further purification. m/z (ES⁺), [M+H]⁺ = 361.

3-(2-(4-fluorophenyl)-6-methylimidazo[1,2-a]pyridin-3-yloxy)propyl methanesulfonate (13e).

To a solution of 3-((2-(4-fluorophenyl)-6-methylimidazo[1,2-a]pyridin-3-yl)oxy)propan-1-ol (1.420 g, 4.73 mmol) in CH₂Cl₂ (20 mL), triethylamine (1.977 mL, 14.18 mmol) was added followed by methanesulfonyl chloride (0.442 mL, 5.67 mmol) at 0 °C and the reaction mixture was allowed to warm to RT and stirred for 3 h. The reaction mixture was transferred to a separatory funnel and washed with Saturated NaHCO₃ followed by brine. The combined organic layer was dried over Na₂SO₄ and evaporated on a rotavap to give a residue which was purified by silica gel column chromatography to give 3-((2-(4-fluorophenyl)-6-methylimidazo[1,2-a]pyridin-3-yl)oxy)propyl methanesulfonate (1.320 g, 73.8%) as a yellowish amorphous powder. m/z (ES⁺), [M+H]⁺ = 379.38.

2-(4-Fluorophenyl)-6-methyl-3-(3-(pyridin-3-yloxy)propoxy)imidazo[1,2-a]pyridine (14e).

To a solution of pyridin-3-ol (0.045 g, 0.48 mmol) in DMF (5 mL), sodium hydride (0.023 g, 0.57 mmol) was added at 0 °C. After stirring for 10 min, 3-((2-(4-fluorophenyl)-6-methylimidazo[1,2-a]pyridin-3-yl)oxy)propyl methanesulfonate (0.18 g, 0.48 mmol) was added and the reaction mixture was stirred at RT for 12 h. The reaction mixture was poured onto ice-water (20 mL) and extracted with EtOAc (20 mL x 3). The combined organic layer was washed with brine and water (20 mL x 3) and dried over Na₂SO₄. The organic layer was concentrated to give a residue which was purified by reverse phase HPLC to give 2-(4-Fluorophenyl)-6-methyl-3-(3-(pyridin-3-yloxy)propoxy)imidazo[1,2-a]pyridine (0.028 g, 15.6%) as an amorphous powder. HRMS *m/z* (M + H)⁺ calculated for [C₂₂H₂₀FN₃O₂ + H]⁺ 378.16115, found 378.1620; ¹H NMR (300 MHz, DMSO-d₆) δ ppm 2.23 (s, 3 H) 2.33 (quin, *J* = 6.03 Hz, 2 H) 4.25 (t, *J* = 6.12 Hz, 2 H) 4.34 (t, *J* = 5.93 Hz, 2 H) 7.02 - 7.17 (m, 3H) 7.33 - 7.49 (m, 3 H) 7.94 - 8.03 (m, 3 H) 8.21 (d, *J* = 4.52 Hz, 1 H) 8.34 (d, *J* = 2.83 Hz, 1 H).

2-(4-Fluorophenyl)-3-(3-((5-fluoropyridin-3-yl)oxy)propoxy)-6-methylimidazo[1,2-a]pyridine (15e).

To a solution of 5-fluoropyridin-3-ol (0.060 g, 0.53 mmol) in DMF (5 mL), sodium hydride (0.025 g, 0.63 mmol) was added at 0 °C. After stirring for 10 min, 3-((2-(4-fluorophenyl)-6-methylimidazo[1,2-a]pyridin-3-yl)oxy)propyl methanesulfonate (0.2 g, 0.53 mmol) was added and the reaction mixture stirred at RT for 12 h. The reaction mixture was poured onto ice-water (20 mL) and extracted with EtOAc (20 mL x 3). The combined organic layer was washed with brine and water (20 mL x 3) and dried over Na₂SO₄. The organic layer was concentrated to give a residue which was purified by reverse phase HPLC to give 2-(4-fluorophenyl)-3-(3-((5-fluoropyridin-3-yl)oxy)propoxy)-6-methylimidazo[1,2-a]pyridine (0.059 g, 28.2%) as an

amorphous powder. HRMS m/z ($M + H$)⁺ calculated for $[C_{22}H_{19}F_2N_3O_2 + H]^+$ 396.15175, found 396.1526; ¹H NMR (300 MHz, DMSO-d₆) δ ppm 2.24 (s, 3 H) 2.33 (quin, $J = 5.93$ Hz, 2 H) 4.23 (t, $J = 6.03$ Hz, 2 H) 4.37 (t, $J = 5.84$ Hz, 2 H) 7.02 - 7.19 (m, 3H) 7.42 (d, $J = 9.23$ Hz, 1 H) 7.53 (dt, $J = 11.21, 2.21$ Hz, 1 H) 7.91 - 8.06 (m, 3 H) 8.17 - 8.29 (m, 2 H).

2-(4-Fluorophenyl)-6-methyl-3-(3-((6-methylpyridin-3-yl)oxy)propoxy)imidazo[1,2-a]pyridine (16e).

To a solution of 6-methylpyridin-3-ol (0.075 g, 0.69 mmol) in DMF (3 mL), sodium hydride (0.025 g, 0.63 mmol) was added at 0 °C. After stirring for 10 min, 3-((2-(4-fluorophenyl)-6-methylimidazo[1,2-a]pyridin-3-yl)oxy)propyl methanesulfonate (0.200 g, 0.53 mmol) was added and the reaction mixture stirred at RT for 12 h. The reaction mixture was poured onto ice-water (20 mL) and extracted with EtOAc (20 mL x 3). The combined organic layer was washed with brine and water (20 mL x 3) and dried over Na₂SO₄. The organic layer was concentrated to give residue which was purified by reverse phase HPLC to give 2-(4-fluorophenyl)-6-methyl-3-(3-((6-methylpyridin-3-yl)oxy)propoxy)imidazo[1,2-a]pyridine (0.115 g, 55.6%) as an amorphous powder. HRMS m/z ($M + H$)⁺ calculated for $[C_{23}H_{22}FN_3O_2 + H]^+$ 392.17685, found 392.1777; ¹H NMR (300 MHz, DMSO-d₆) δ ppm 2.23 (s, 3 H) 2.31 (t, $J = 6.03$ Hz, 2 H) 2.41 (s, 3 H) 4.23 (t, $J = 5.93$ Hz, 2 H) 4.29 (t, $J = 5.84$ Hz, 2 H) 7.04 - 7.17 (m, 3H) 7.21 (d, $J = 8.48$ Hz, 1 H) 7.35 (dd, $J = 8.48, 2.83$ Hz, 1 H) 7.42 (d, $J = 9.04$ Hz, 1 H) 7.94 - 8.04 (m, 3 H) 8.20 (d, $J = 2.45$ Hz, 1 H).

3-(3-((2,6-Dimethylpyridin-3-yl)oxy)propoxy)-2-(4-fluorophenyl)-6-methylimidazo[1,2-a]pyridine (17e).

To a solution of 2,6-dimethylpyridin-3-ol (0.123 g, 1.00 mmol) in DMF (5 mL), sodium hydride (0.037 g, 0.92 mmol) was added at 0 °C. After stirring for 10 min, 3-((2-(4-fluorophenyl)-6-methylimidazo[1,2-a]pyridin-3-yl)oxy)propyl methanesulfonate (0.290 g, 0.77 mmol) was added and the reaction mixture was stirred at RT for 12 h. The reaction mixture was poured onto ice-water (20 mL) and extracted with EtOAc (20 mL x 3). The combined organic layer was washed with brine and water (20 mL x 3) and dried over Na₂SO₄. The organic layer was concentrated to give a residue which was purified by reverse phase HPLC to give 3-(3-((2,6-dimethylpyridin-3-yl)oxy)propoxy)-2-(4-fluorophenyl)-6-methylimidazo[1,2-a]pyridine (0.145 g, 46.7%) as an amorphous powder. HRMS m/z (M + H)⁺ calculated for [C₂₄H₂₄FN₃O₂ + H]⁺ 406.19245, found 406.1884; ¹H NMR (300 MHz, DMSO-*d*₆) δ ppm 2.21 (d, *J* = 5.27 Hz, 6 H) 2.26 - 2.35 (m, 2 H) 2.37 (s, 3 H) 4.25 (t, *J* = 5.65 Hz, 4 H) 7.00 - 7.12 (m, 4 H) 7.31 (d, *J* = 8.29 Hz, 1 H) 7.42 (d, *J* = 9.23 Hz, 1 H) 7.91 - 8.01 (m, 3 H).

6-Methyl-3-(3-(4-methylpiperazin-1-yl)propoxy)-2-phenylimidazo[1,2-a]pyridine (18d).

A solution of 3-(3-bromopropoxy)-6-methyl-2-phenylimidazo[1,2-a]pyridine (0.308 g, 0.89 mmol) and 1-methylpiperazine (0.298 mL, 2.68 mmol) in DMF (5 mL) was stirred at RT for 16 h. The reaction mixture was diluted with EtOAc (40 mL) and washed with brine (30 mL x 2). The organic layer was dried over Na₂SO₄ and evaporated in a rotavap to give a residue which was purified by reverse phase HPLC to give 6-methyl-3-(3-(4-methylpiperazin-1-yl)propoxy)-2-phenylimidazo[1,2-a]pyridine (0.093 g, 28.6 %) as an oily liquid. HRMS m/z (M + H)⁺ calculated for [C₂₂H₂₈N₄O + H]⁺ 365.23355, found 365.2340; ¹H NMR (300 MHz, DMSO-*d*₆) δ ppm 1.99 (t, *J* = 6.40 Hz, 2 H) 2.15 (s, 3 H) 2.21 - 2.60 (m, 13 H) 4.10 (t, *J* = 6.03 Hz, 2 H) 7.07 (d, *J* = 8.85 Hz, 1 H) 7.25 - 7.35 (m, 1 H) 7.38 - 7.52 (m, 3 H) 7.96 - 8.11 (m, 3 H).

4-Fluoro-N-(3-((2-(4-fluorophenyl)-6-methylimidazo[1,2-a]pyridin-3-yl)oxy)propyl)-3-methylaniline (19e).

To a solution of 3-((2-(4-fluorophenyl)-6-methylimidazo[1,2-a]pyridin-3-yl)oxy)propyl methanesulfonate (0.180 g, 0.48 mmol) and 4-fluoro-3-methylaniline (0.119 g, 0.95 mmol) in toluene (5 mL), N,N-diisopropylethylamine (0.166 mL, 0.95 mmol) was added and the reaction mixture refluxed for 12 h. The reaction mixture was transferred to a separatory funnel and washed with brine. The combined organic layer was dried over Na₂SO₄ and evaporated in a rotavap to give a residue which was purified by reverse phase HPLC to give 4-fluoro-N-(3-((2-(4-fluorophenyl)-6-methylimidazo[1,2-a]pyridin-3-yl)oxy)propyl)-3-methylaniline (0.052 g, 26.8%) as a liquid. HRMS *m/z* (M + H)⁺ calculated for [C₂₄H₂₃F₂N₃O + H]⁺ 408.18815, found 408.1846; ¹H NMR (300 MHz, DMSO-*d*₆) δ ppm 2.10 - 2.19 (m, 5 H) 2.22 (s, 3 H) 3.23 (q, *J* = 6.09 Hz, 2 H) 4.19 (t, *J* = 6.03 Hz, 2 H) 5.50 (t, *J* = 5.27 Hz, 1 H) 6.37 - 6.52 (m, 2 H) 6.88 (t, *J* = 9.23 Hz, 1 H) 7.03 - 7.10 (m, 1 H) 7.18 (t, *J* = 8.95 Hz, 2 H) 7.41 (d, *J* = 9.04 Hz, 1 H) 7.96 - 8.06 (m, 3 H).

5-Fluoro-N-(3-((2-(4-fluorophenyl)-6-methylimidazo[1,2-a]pyridin-3-yl)oxy)propyl)-6-methylpyridin-2-amine (20e).

To a solution of 3-((2-(4-fluorophenyl)-6-methylimidazo[1,2-a]pyridin-3-yl)oxy)propyl methanesulfonate (0.235 g, 0.62 mmol) and 5-fluoro-6-methylpyridin-2-amine (0.094 g, 0.75 mmol) in toluene (5 mL), N,N-diisopropylethylamine (0.217 mL, 1.24 mmol) was added and the reaction mixture refluxed for 16 h. The reaction mixture was transferred to a separatory funnel and washed with saturated NaHCO₃ followed by brine. The combined organic layer was dried

over Na₂SO₄ and evaporated in a rotavap to give a residue which was purified by silica gel column chromatography to give 5-fluoro-N-(3-((2-(4-fluorophenyl)-6-methylimidazo[1,2-a]pyridin-3-yl)oxy)propyl)-6-methylpyridin-2-amine (0.022 g, 8.7) as a yellowish amorphous powder. HRMS *m/z* (M + H)⁺ calculated for [C₂₃H₂₂F₂N₄O + H]⁺ 409.18345, found 409.1841; ¹H NMR (300 MHz, DMSO-*d*₆) δ ppm 2.11 (t, *J* = 6.40 Hz, 2 H) 2.25 (s, 6 H) 3.43 (q, *J* = 6.34 Hz, 2 H) 4.16 (t, *J* = 6.22 Hz, 2 H) 6.32 (dd, *J* = 8.85, 2.45 Hz, 1 H) 6.48 (t, *J* = 5.09 Hz, 1 H) 7.07 (d, *J* = 9.42 Hz, 1 H) 7.13 - 7.34 (m, 3 H) 7.41 (d, *J* = 9.23 Hz, 1 H) 7.95 - 8.07 (m, 3 H).

2-(4-Fluorophenyl)-6-methyl-3-(3-(4-phenylpiperazin-1-yl)propoxy)imidazo[1,2-a]pyridine (21e).

A solution of 3-((2-(4-fluorophenyl)-6-methylimidazo[1,2-a]pyridin-3-yl)oxy)propyl methanesulfonate (0.233 g, 0.62 mmol) and 1-phenylpiperazine (0.282 mL, 1.85 mmol) in DMF (5 mL) was stirred at RT for 96 h. The reaction mixture was diluted with EtOAc (40 mL) and washed with brine (30 mL x 2). The organic layer was dried over Na₂SO₄ and evaporated in a rotavap to give a residue which was purified by reverse phase HPLC to give 2-(4-fluorophenyl)-6-methyl-3-(3-(4-phenylpiperazin-1-yl)propoxy)imidazo[1,2-a]pyridine (0.100 g, 36.5%) as a white amorphous powder. HRMS *m/z* (M + H)⁺ calculated for [C₂₇H₂₉FN₄O + H]⁺ 445.23975, found 445.2354; ¹H NMR (300 MHz, DMSO-*d*₆) δ ppm 1.96 - 2.13 (m, 2 H) 2.31 (s, 3 H) 2.55 (br. s., 6 H) 3.13 (br. s., 4 H) 4.13 (t, *J* = 6.03 Hz, 2 H) 6.77 (t, *J* = 7.06 Hz, 1 H) 6.93 (d, *J* = 8.10 Hz, 2 H) 7.07 (d, *J* = 8.29 Hz, 1 H) 7.16 - 7.35 (m, 4 H) 7.42 (d, *J* = 9.23 Hz, 1 H) 7.98 - 8.13 (m, 3 H).

N-(3-((2-(4-Fluorophenyl)-6-methylimidazo[1,2-a]pyridin-3-yl)oxy)propyl)-6-methoxy-5-methylpyridin-3-amine (22e).

To a solution of 3-((2-(4-fluorophenyl)-6-methylimidazo[1,2-a]pyridin-3-yl)oxy)propyl methanesulfonate (0.192 g, 0.51 mmol) and 6-methoxy-5-methylpyridin-3-amine (0.084 g, 0.61 mmol) in toluene (2 mL), *N,N*-diisopropylethylamine (0.177 mL, 1.01 mmol) was added and the reaction mixture refluxed for 6 h. The reaction mixture was transferred to a separatory funnel and washed with saturated NaHCO_3 followed by brine. The combined organic layer was dried over Na_2SO_4 and evaporated in a rotavap to give a residue which was purified by silica gel column chromatography to give N-(3-((2-(4-fluorophenyl)-6-methylimidazo[1,2-a]pyridin-3-yl)oxy)propyl)-6-methoxy-5-methylpyridin-3-amine (0.071 g, 33.3%) as a yellowish amorphous powder. HRMS m/z ($M + H$)⁺ calculated for $[\text{C}_{24}\text{H}_{25}\text{FN}_4\text{O}_2 + H]^+$ 421.20335, found 421.1972; ¹H NMR (300 MHz, DMSO-*d*₆) δ ppm 2.08 (s, 3 H) 2.09 - 2.17 (m, 2 H) 2.23 (s, 3 H) 3.23 (q, J = 6.40 Hz, 2 H) 3.75 (s, 3 H) 4.19 (t, J = 6.03 Hz, 2 H) 5.28 (t, J = 5.56 Hz, 1 H) 6.94 (d, J = 2.26 Hz, 1 H) 7.06 (d, J = 9.23 Hz, 1 H) 7.19 (t, J = 8.85 Hz, 2 H) 7.35 - 7.45 (m, 2 H) 7.97 - 8.06 (m, 3 H).

5-Bromo-N-(3-((2-(4-fluorophenyl)-6-methylimidazo[1,2-a]pyridin-3-yl)oxy)propyl)-6-methylpyridin-3-amine (23e).

To a solution of 3-((2-(4-fluorophenyl)-6-methylimidazo[1,2-a]pyridin-3-yl)oxy)propyl methanesulfonate (0.192 g, 0.51 mmol) and 5-bromo-6-methylpyridin-3-amine (0.114 g, 0.61 mmol) in toluene (2 mL), *N,N*-diisopropylethylamine (0.177 mL, 1.01 mmol) was added and the reaction mixture refluxed for 16 h. The reaction mixture was transferred to a separatory funnel and washed with saturated NaHCO_3 followed by brine. The combined organic layer was dried

over Na₂SO₄ and evaporated in a rotavap to give a residue which was purified by silica gel column chromatography to give 5-bromo-N-(3-((2-(4-fluorophenyl)-6-methylimidazo[1,2-a]pyridin-3-yl)oxy)propyl)-6-methylpyridin-3-amine (0.023 g, 9.7%) as a gum. HRMS *m/z* (*M* + *H*)⁺ calculated for [C₂₃H₂₂BrN₄O + *H*]⁺ 469.10335, found 469.1006; ¹H NMR (300 MHz, DMSO-*d*₆) δ ppm 2.11 (t, *J* = 6.50 Hz, 2 H) 2.25 (s, 3 H) 2.41 (s, 3 H) 3.28 (d, *J* = 5.84 Hz, 2 H) 4.18 (t, *J* = 5.93 Hz, 2 H) 6.01 - 6.09 (m, 1 H) 7.07 (d, *J* = 7.91 Hz, 1 H) 7.15 - 7.24 (m, 3 H) 7.42 (d, *J* = 9.23 Hz, 1 H) 7.90 (d, *J* = 2.26 Hz, 1 H) 7.98 - 8.03 (m, 3 H).

4-Fluoro-N-(3-((2-(4-fluorophenyl)-6-methylimidazo[1,2-a]pyridin-3-yl)oxy)propyl)benzenesulfonamide (24e).

Aqueous ammonia (11.32 mL, 523.23 mmol) was added to 3-((2-(4-fluorophenyl)-6-methylimidazo[1,2-a]pyridin-3-yl)oxy)propyl methanesulfonate (0.792 g, 2.09 mmol) and the resulting suspension was heated to 100 °C in a steel bomb for 16 h. The reaction mixture was transferred to a separatory funnel and extracted with DCM (20 mL x 2). The combined organic layer was dried over Na₂SO₄ and evaporated in a rotavap to give a residue (0.250 g, 39.9%) which was used directly for the next step without further purification. ESI *m/z* (*ES*⁺), [*M*+*H*]⁺ = 300. To a solution of 3-((2-(4-fluorophenyl)-6-methylimidazo[1,2-a]pyridin-3-yl)oxy)propan-1-amine (0.200 g, 0.67 mmol) in DCM (10 mL), 4-fluorobenzene-1-sulfonyl chloride (0.156 g, 0.80 mmol) was added at 0 °C and the reaction mixture was allowed to warm to RT and stirred for 12 h. The reaction mixture was transferred to a separatory funnel and washed with saturated NaHCO₃ followed by brine. The combined organic layer was dried over Na₂SO₄ and evaporated in a rotavap to give a residue which was purified by reverse phase HPLC to give 4-fluoro-N-(3-((2-(4-fluorophenyl)-6-methylimidazo[1,2-a]pyridin-3-

yl)oxy)propyl)benzenesulfonamide (0.153 g, 50.1%) as an amorphous powder. HRMS m/z ($M + H$)⁺ calculated for $[C_{23}H_{21}F_2N_3O_3S + H]^+$ 458.13445, found 458.1337; ¹H NMR (300 MHz, DMSO-*d*₆) δ ppm 1.96 (t, $J = 6.40$ Hz, 2 H) 2.32 (s, 3 H) 3.01 (q, $J = 6.53$ Hz, 2 H) 4.08 (t, $J = 6.22$ Hz, 2 H) 7.09 (d, $J = 8.10$ Hz, 1H) 7.27 (t, $J = 8.95$ Hz, 2 H) 7.39 - 7.50 (m, 3 H) 7.79 (t, $J = 5.65$ Hz, 1 H) 7.88 (dd, $J = 8.85, 5.27$ Hz, 2 H) 7.96 - 8.08 (m, 3 H).

2-(2-(4-Fluorophenyl)-6-methylimidazo[1,2-a]pyridin-3-yloxy)ethanol (25e).

2-(4-Fluorophenyl)-6-methylimidazo[1,2-a]pyridin-3-ol (1.344 g, 5.55 mmol), 2-bromo-ethanol (0.392 mL, 5.55 mmol) and potassium carbonate (3.83 g, 27.74 mmol) were stirred together in DMF (5 mL) under N₂ at RT for 16 h. The reaction mixture was quenched by adding water (20 mL) and extracted with EtOAc (30 mL x 3). The combined organic layer was washed with brine (30 mL x 3) and dried over Na₂SO₄. The material was evaporated in a rotavap and the residue was purified by column chromatography to give liquid 2-((2-(4-fluorophenyl)-6-methylimidazo[1,2-a]pyridin-3-yl)oxy)ethanol (0.440 g, 27.7 %). ESI m/z (ES⁺), $[M+H]^+ = 287.10$.

3-(2-Azidoethoxy)-2-(4-fluorophenyl)-6-methylimidazo[1,2-a]pyridine (26e).

A solution of 2-((2-(4-fluorophenyl)-6-methylimidazo[1,2-a]pyridin-3-yl)oxy)ethanol (0.440 g, 1.54 mmol) in anhydrous tetrahydrofuran (23 mL) was cooled to 0 °C, and triphenylphosphine (0.806 g, 3.07 mmol) was added at once. After 5 min of stirring, diisopropyl azodicarboxylate (0.598 mL, 3.07 mmol) and subsequently diphenyl phosphorazidate (0.846 g, 3.07 mmol) were added, the ice bath was removed, and the resulting mixture was stirred from 0 °C to RT for 16 h. Volatile material was removed by rotavap and the resulting residue purified by column

chromatography to get 3-(2-azidoethoxy)-2-(4-fluorophenyl)-6-methylimidazo[1,2-a]pyridine (0.300 g, 62.7%) as a liquid. m/z (ES⁺), $[M+H]^+ = 312.36$.

2-(2-(4-Fluorophenyl)-6-methylimidazo[1,2-a]pyridin-3-yloxy)ethanamine (27e).

A solution of 3-(2-azidoethoxy)-2-(4-fluorophenyl)-6-methylimidazo[1,2-a]pyridine (0.30 g, 0.96 mmol) and triphenylphosphine (0.303 g, 1.16 mmol) in THF (4 mL) and water (0.50 mL) was allowed to stir for 18 h at room temperature. The solvent was removed under vacuum to give residue which was purified on neutral alumina column to give 2-(2-(4-Fluorophenyl)-6-methylimidazo[1,2-a]pyridin-3-yloxy)ethanamine (0.217 g, 79%) as a liquid. ESI m/z (ES⁺), $[M+H]^+ = 286.11$.

N-(3-Fluoro-4-methylbenzyl)-2-((2-(4-fluorophenyl)-6-methylimidazo[1,2-a]pyridin-3-yl)oxy)ethanamine (28e).

To a solution of 2-((2-(4-fluorophenyl)-6-methylimidazo[1,2-a]pyridin-3-yl)oxy)ethanamine (54 mg, 0.19 mmol) and 3-fluoro-4-methylbenzaldehyde (26.1 mg, 0.19 mmol) in DCM (2 mL), sodium triacetoxyborohydride (100 mg, 0.47 mmol) was added at RT and stirred for 24 h. The reaction mixture was worked up and the residue purified by reverse phase HPLC to give N-(3-fluoro-4-methylbenzyl)-2-((2-(4-fluorophenyl)-6-methylimidazo[1,2-a]pyridin-3-yl)oxy)ethanamine (15.00 mg, 19.5%) as a liquid. HRMS m/z ($M + H$)⁺ calculated for $[C_{24}H_{23}F_2N_3O + H]^+$ 408.18815, found 408.1856; ¹H NMR (300 MHz, DMSO-*d*₆) δ ppm 2.23 (s, 3 H) 2.30 (s, 3 H) 3.10 (br. s., 2 H) 3.93 (br. s., 2 H) 4.19 (br. s., 2 H) 6.33 (s, 1 H) 6.56 (s, 1 H) 7.05 - 7.33 (m, 5 H) 7.43 (d, $J = 9.42$ Hz, 1 H) 8.06 (dd, $J = 8.38, 5.75$ Hz, 2 H) 8.17 (s, 1 H).

3-Chloro-4-fluoro-N-(2-((2-(4-fluorophenyl)-6-methylimidazo[1,2-a]pyridin-3-yl)oxy)ethyl)benzenesulfonamide (29e).

To a solution of 2-((2-(4-fluorophenyl)-6-methylimidazo[1,2-a]pyridin-3-yl)oxy)ethanamine (58 mg, 0.20 mmol) in CH₂Cl₂ (4 mL), triethylamine (0.085 mL, 0.61 mmol) was added followed by 3-chloro-4-fluorobenzene-1-sulfonyl chloride (51.2 mg, 0.22 mmol) at 0 °C. The reaction mixture was allowed to warm to RT and stirred for 16 h. The reaction mixture was worked up and the residue was purified by reverse phase HPLC to give 3-chloro-4-fluoro-N-(2-((2-(4-fluorophenyl)-6-methylimidazo[1,2-a]pyridin-3-yl)oxy)ethyl)benzenesulfonamide (36.0 mg, 37.1%) as an amorphous powder. HRMS *m/z* (M + H)⁺ calculated for [C₂₂H₁₈ClF₂N₃O₃S + H]⁺ 478.07975, found 478.0812; ¹H NMR (300 MHz, DMSO-*d*₆) δ ppm 2.32 (s, 3 H) 3.33 (m, 2 H) 4.05 (t, *J* = 4.90 Hz, 2 H) 7.09 (d, *J* = 8.10 Hz, 1 H) 7.25 (t, *J* = 8.85 Hz, 2 H) 7.42 (d, *J* = 9.23 Hz, 1H) 7.60 - 7.69 (m, 1 H) 7.82 - 7.89 (m, 1 H) 7.98 - 8.07 (m, 3 H) 8.09 (s, 1 H) 8.37 (br. s., 1 H).

N-(2-((2-(4-Fluorophenyl)-6-methylimidazo[1,2-a]pyridin-3-yl)oxy)ethyl)-6-methylnicotinamide (30e).

To a solution of 2-((2-(4-fluorophenyl)-6-methylimidazo[1,2-a]pyridin-3-yl)oxy)ethanamine (88 mg, 0.31 mmol) in CH₂Cl₂ (2 mL), triethylamine (0.129 mL, 0.93 mmol) was added followed by 6-methylnicotinoyl chloride (57.6 mg, 0.37 mmol) at 0 °C. The resulting reaction mixture was allowed to warm to RT and stirred for 12 h. The reaction mixture was quenched with saturated NaHCO₃ (10 mL) and extracted with DCM (25 mL x 3). The combined organic layer was dried over Na₂SO₄ and evaporated in a rotavap to give a residue which was purified by reverse phase HPLC to give N-(2-((2-(4-fluorophenyl)-6-methylimidazo[1,2-a]pyridin-3-yl)oxy)ethyl)-6-

methylnicotinamide (73.0 mg, 58.5 %) as a white amorphous powder. HRMS m/z ($M + H$)⁺ calculated for $[C_{23}H_{21}FN_4O_2 + H]^+$ 405.17205, found 405.1724; ¹H NMR (300 MHz, DMSO-*d*₆) δ ppm 2.20 (s, 3 H) 2.55 (s, 3 H) 3.77 (d, J = 4.90 Hz, 2 H) 4.22 (t, J = 5.09 Hz, 2 H) 6.99 - 7.10 (m, 3 H) 7.41 (d, J = 8.67 Hz, 2 H) 7.96 - 8.08 (m, 3 H) 8.15 (dd, J = 8.10, 2.26 Hz, 1 H) 8.97 (d, J = 2.07 Hz, 1 H) 9.08 (s, 1 H).

General procedure for squaramides demonstrated with compound 31g

3-(Benzylamino)-4-(4-morpholinophenyl)cyclobut-3-ene-1,2-dione (31g)

Step 1. 3-Chloro-4-(4-morpholinophenyl)cyclobut-3-ene-1,2-dione (31b).

A mixture of 3,4-dihydroxycyclobut-3-ene-1,2-dione (1 g, 8.77 mmol), thionyl chloride (1.280 mL, 17.54 mmol) and DMF (3 drops) was refluxed at 80 °C for 3 h. Formation of dichloride could not be followed by LCMS. The reaction mixture was cooled to room temperature and excess thionyl chloride was evaporated under reduced pressure. The residual mass was re-dissolved in anhydrous DCM (10 mL) and cooled to 0 °C. Anhydrous AlCl₃ (0.529 g, 2.19 mmol) was carefully added followed by dropwise addition of 4-phenylmorpholine (1.431 g, 8.77 mmol). Throughout the addition, temperature was maintained at 0 °C. After completion of addition, the temperature was allowed to warm to room temperature and stirring continued for additional 1.5 h. Formation of product was followed by LCMS. After completion of the reaction, the mixture was poured onto crushed ice and the crude product was extracted into DCM (2 X 20 mL). The combined organic layer was washed with water (15 mL), brine (15 mL), dried over Na₂SO₄ and evaporated under reduced pressure. Purification of crude product through combiflash chromatography with preloaded silica gel column using ethylacetate-hexane gradient resulted in 0.400g of pure 3-chloro-4-(4-morpholinophenyl)cyclobut-3-ene-1,2-dione in 16%

yield. ^1H NMR (300 MHz, CHCl_3) δ ppm 3.28 - 3.43 (m, 2 H), 3.70 - 3.91 (m, 2 H), 6.79 - 6.97 (m, 1 H), 8.11 (d, $J=9.0$ Hz, 1 H), ESMS calcd. 277.7; Found: 278.2 (M^+) $^+$.

Step 2. 3-(Benzylamino)-4-(4-morpholinophenyl)cyclobut-3-ene-1,2-dione (31g).

A solution of 3-chloro-4-(4-morpholinophenyl)cyclobut-3-ene-1,2-dione **31b** (0.100 g, 0.36 mmol) dissolved in dioxane (10 mL) was cooled to 0-5 $^\circ\text{C}$. At that temperature, TEA (0.075 mL, 0.54 mmol) was added followed by addition of phenylmethanamine (0.058 g, 0.54 mmol). Stirring was continued for another 10 min after addition. Solvent was evaporated and the residue was triturated with water (5 mL) and the separated solid was filtered and air dried. Purification of crude product through combiflash chromatography with preloaded silica gel column using Methanol-DCM gradient resulted in 0.07g of pure 3-(benzylamino)-4-(4-morpholinophenyl)cyclobut-3-ene-1,2-dione **31d** as yellowish amorphous powder in 55.8% yield. ^1H NMR (300 MHz, $\text{DMSO}-d_6$) δ ppm 3.28 (d, $J=4.3$ Hz, 4 H), 3.67 - 3.80 (m, 4 H), 4.90 (d, $J=6.2$ Hz, 2 H), 7.06 (d, $J=8.8$ Hz, 2 H), 7.26 - 7.35 (m, 1 H), 7.35 - 7.40 (m, 4 H), 7.94 (d, $J=8.6$ Hz, 2 H), 9.35 (t, 1 H), HRMS (ES+) m/z calcd for $[\text{C}_{21}\text{H}_{20}\text{N}_2\text{O}_3 + \text{H}]^+$ 349.1552; found: 349.1550.

3-(Pyridin-2-ylmethylamino)-4-(4-(trifluoromethyl)phenyl)cyclobut-3-ene-1,2-dione (31c).

Yield: 40.1%. ^1H NMR (300 MHz, $\text{DMSO}-d_6$) δ ppm 5.04 (d, $J=6.2$ Hz, 2 H), 7.28 - 7.39 (m, 1 H), 7.48 (d, $J=8.1$ Hz, 1 H), 7.78 - 7.87 (m, 1 H), 7.91 (d, $J=8.30$ Hz, 2 H), 8.22 (d, $J=8.1$ Hz, 2 H), 8.56 (d, $J=4.5$ Hz, 1 H), 9.92 (t, $J=6.1$ Hz, 1 H), 10.60 - 10.70 (m, 1 H), HRMS (ES+) m/z calcd for $[\text{C}_{17}\text{H}_{11}\text{F}_3\text{N}_2\text{O}_2 + \text{H}]^+$ 333.0845; found: 333.0839.

3-((5-Methylpyrazin-2-yl)methylamino)-4-(4-(trifluoromethyl)phenyl)cyclobut-3-ene-1,2-dione (31d).

Yield: 36.7%. ¹H NMR (300 MHz, DMSO-*d*₆) δ ppm 2.55 (s, 3H), 5.27 (d, *J*=6.1 Hz, 2 H), 7.89 (d, *J*=8.0 Hz, 2 H), 8.02 (d, *J*=8.10 Hz, 2 H), 8.42 (s, 1H), 8.59 (s, 1 H) 10.80 - 11.00 (t, *J*= 6.0 Hz, 1 H), HRMS (ES+) *m/z* calcd for [C₁₇H₁₂F₃N₃O₂+ H]⁺ 348.09600; found: 348.0971.

4-(3,4-Dioxo-2-(pyridin-2-ylmethylamino)cyclobut-1-enyl)benzonitrile (31e).

Yield 50.5%. ¹H NMR (300 MHz, DMSO-*d*₆) δ ppm 5.08 (d, *J*=6.20 Hz, 2 H), 7.22 (t, *J*=9.0 Hz, 1H), 7.48 (dd, *J*= 8.0Hz, 6.0Hz, 1H), 7.68 (t, *J*=8.0Hz, 1H), 7.72 (d, *J*=8.44 Hz, 2 H), 7.85 (d, *J*=8.22 Hz, 2 H), 8.59 (d, *J*=5.15 Hz, 1 H), 9.30 (t, *J*= 6.2Hz, 1 H), HRMS (ES+) *m/z* calcd for [C₁₇H₁₁N₃O₂+ H]⁺ 290.0930; found: 290.0930.

3-(4-Morpholinophenyl)-4-((pyridin-2-ylmethyl)amino)cyclobut-3-ene-1,2-dione (31f).

Yield: 16.1%. ¹H NMR (300 MHz, DMSO-*d*₆) δ ppm 3.24 - 3.32 (m, 4 H), 3.70 - 3.79 (m, 4 H), 5.01 (d, *J*=6.22 Hz, 2 H), 7.07 (d, *J*=8.85 Hz, 2 H), 7.32 (dd, *J*=6.7, 5.09 Hz, 1 H), 7.43 (d, *J*=7.9 Hz, 1 H), 7.76 - 7.86 (m, 1 H), 7.96 (d, *J*=8.8 Hz, 2 H), 8.55 (d, *J*=4.52 Hz, 1 H), 9.41 (t, *J*=6.1 Hz, 1 H), HRMS (ES+) *m/z* calcd for [C₂₀H₁₉N₃O₃+ H]⁺ 350.1498; found: 350.1500.

3-(4-Morpholinophenyl)-4-((1-(pyridin-2-yl)ethyl)amino)cyclobut-3-ene-1,2-dione (31h).

Yield 46.7%. ¹H NMR (DMSO-*d*₆, 300MHz): δ (ppm) 1.68 (d, *J*=7.0 Hz, 3H), 3.23 - 3.30 (m, 4H), 3.64 - 3.82 (m, 4H), 5.61 - 5.77 (m, 1H), 7.07 (d, *J*=8.9 Hz, 2H), 7.32 (dd, *J*=7.2, 5.3 Hz, 1H), 7.49 (d, *J*=7.9 Hz, 1H), 7.77 - 7.87 (m, 1H), 8.01(d, *J*=8.9 Hz, 2H), 8.57 (d, *J*=4.1 Hz, 1H),

9.22 (d, $J=8.5$ Hz, 1H), HRMS (ES+) m/z calcd for $[C_{21}H_{21}N_3O_3 + H]^+$ 364.1661; found: 364.1575.

3-(4-Morpholinophenyl)-4-((pyrazin-2-ylmethyl)amino)cyclobut-3-ene-1,2-dione (31i).

Yield: 27.7%. 1H NMR (300 MHz, DMSO- d_6) δ ppm 3.27 - 3.31 (m, 4 H), 3.71 - 3.81 (m, 4 H), 5.07 (d, $J=6.0$ Hz, 2 H), 7.07 (d, $J=8.8$ Hz, 2 H), 7.93 (d, $J=8.8$ Hz, 2 H), 8.54 - 8.67 (m, 2 H), 8.75 (s, 1 H), 9.36 (t, $J=5.9$ Hz, 1 H), HRMS (ES+) m/z calcd for $[C_{19}H_{18}N_4O_3 + H]^+$ 351.1451; found: 351.1448.

3-(4-Morpholinophenyl)-4-(((5-phenylpyridin-2-yl)methyl)amino)cyclobut-3-ene-1,2-dione (31j).

Yield: 53.4%. 1H NMR (DMSO- d_6 , 300MHz): δ (ppm) 3.29 (t, $J=4.5$ Hz, 4H), 3.68 - 3.79 (m, 4H), 5.06 (d, $J=6.2$ Hz, 2H), 7.08 (d, $J=8.9$ Hz, 2H), 7.37 - 7.56 (m, 4H), 7.73 (d, $J=7.3$ Hz, 2H), 7.97 (d, $J=8.9$ Hz, 2H), 8.11 (dd, $J=8.2, 2.4$ Hz, 1H), 8.88 (d, $J=2.1$ Hz, 1H), 9.43 (t, $J=5.9$ Hz, 1H), HRMS (ES+) m/z calcd for $[C_{26}H_{23}N_3O_3 + H]^+$ 426.1811; found: 426.1815.

ACKNOWLEDGMENT

We sincerely thank Compound management group (AstraZeneca R&D Bangalore), DMPK (AstraZeneca, Waltham, USA), and Global Discovery Sciences, Safety (AstraZeneca, Alderley Park, UK) for technical support. We acknowledge Sandeep Ghorpade and Pravin Shirude for scientific discussions. We also thank Drs. R. Tommasi and T. S. Balganesh for their constant inspiration, support, and encouragement. We also thank the support received from Drs. Prashanti

Madhavapeddi, Beena Paul towards assay development and Dr. Dwarakanath Prahlad towards data management during the study.

AUTHOR CONTRIBUTION

S.J.T., S.D.M., A.R., C.C., P.I., M.P. and S.H.P. are responsible for medicinal chemistry design and analyses. S.J.T., S.D.M., V.S. and C.K. are responsible for synthetic chemistry. S.R. and M.M are responsible for compound purity. A.K.G and M.P. designed and performed the modelling studies. S.H.P., K.M., M.P., S.K., M.M. and V.B. performed hit triage for the high through screen output. K.R., D. M., H.P., M.P., H.A., D.P., J.W., P.A., K.N. and M.C. performed high throughput screening. K.M., H.R., T.Y. and K.M. designed IC₅₀ determination experiments. G.B. and J.B. performed and analysed the IC₅₀ determination experiments. H.R. and T.I. designed, performed and analyzed biochemical deconvolution experiments and data. V.R., V.K.S., K.M., V.B. and S.R. designed the microbiology experiments. A.N., S.S., P.K., N.D., S.G., performed microbiology experiments. V.P.H., S.S., S.N. and R.K.S. designed and analysed PK-PD experiments. N.K., R.N., S.B., J.R., V.P., P.K.R., K.K. and R.S. performed PK-PD experiments. S.R., N.V.M., A.A. and V.K.S. designed and performed mutant generation experiments. J.W. and R.E.M. performed and analysed Whole genome sequencing and data analysis. S.J.T., S.D.M., A.K.G., S.R. and S.H.P wrote the manuscript with contributions from all co-authors.

ABBREVIATIONS

TB, tuberculosis; *Mtb*, *Mycobacterium tuberculosis*; *Msm*, *Mycobacterium smegmatis*; MIC, minimum inhibitory concentration; HB, H-bond; SAR, structure-activity relationship; SPR, structure property relationship; AUC, Area under the curve; f, free fraction; QD, once a day;

BID, twice a day; CFU, colony forming units; RT, room temperature; DME, 1,2-dimethoxyethane; THF, tetrahydrofuran; DMF, N,N-dimethylformamide; ABT, aminobenzotriazole; BSL-3, Biosafety level 3 laboratory; Ox-phos, Oxidative phosphorylation; HTS, High throughput Screening; LHS, Left hand side; RHS, Right hand side; THNA, tetrahydronaphthylamines; SQA, Squaramides; IPE, Imidazolo pyridine ethers; IMV, Inverted membrane vesicles; SMP_ATPS, Mitochondrial ATP synthesis assay; Myc_ATPS, Mycobacterial ATP synthesis assay.

SUPPORTING INFORMATION

Tables with data on specificity and selectivity of SQA and IPE compounds, specificity of growth inhibition, MBCs of IPE compounds, SNPs in SQA mutants, *M. smegmatis* MIC for IPEs, Cross resistance profile of IPE & SQA compounds, Figures of sequence alignment of *M. tuberculosis* subunit-*a* of ATP synthase with subunit-*a* of *E. coli* ATP synthase and 2D interaction diagram of SQA ligands with *M. tuberculosis* ATP synthase. pdb files of mycobacterium ATP synthase with ligands and a csv file with molecular string formula and biological data.

AUTHOR INFORMATION

*Corresponding Author

Email and Phone numbers

shahulhameed@bugworksresearch.com

+91 9945 699089

mailsuravi01@gmail.com

+91 9845 537810

REFERENCES

1. http://apps.who.int/iris/bitstream/10665/191102/1/9789241565059_eng.pdf, Global tuberculosis report 2015, 20th edition, WHO Oct 7, **2015**.
2. Dye. C.; Williams, B. G. The population dynamics and control of tuberculosis. *Science* **2010**, 328, 856–861.
3. Zumla, A.; Raviglione, M.; Hafner. R.; von Reyn. C. F. Tuberculosis. *N. Eng. J. Med.* **2013**, 368, 745-755.
4. Gandhi, N. R.; Nunn, P.; Dheda, K.; Schaaf, H. S.; Zignol, M.; van Soolingen, D.; Jensen, P.; Bayona, J. Multidrug-resistant and extensively drug-resistant tuberculosis: A threat to global control of tuberculosis. *Lancet* **2010**, 375, 1830–1843.
5. Mandavilli, A. Virtually incurable TB warns of impending disaster. *Nat. Med.* **2007**, 13, 271-271.
6. http://www.who.int/tb/features_archive/m_xdrtb_facts/en/, Multidrug and extensively drug-resistant TB (M/XDR-TB): 2010 global report on surveillance and response. WHO **2010**.
7. Mitchison, D. A. The diagnosis and therapy of tuberculosis during the past 100 years. *Am. J. Respir. Crit. Care Med.* **2005**, 171, 699–706.
8. Tsara, S.; Serasli, E.; Christaki, P. Problems in diagnosis and treatment of tuberculosis infection. *Hippokratia* **2009**, 13, 20-22.
9. Russel, D. G.; Barry, III, C. E.; Flynn, J. L. Tuberculosis: What we don't know can, and does, hurt us. *Science* **2010**, 328, 852–856.

10. Horsburgh Jr. C.R.; Barry III, C.E.; Lange, C. Treatment of tuberculosis, *N. Engl. J. Med.* **2015**, *373*, 2149-2160.
11. Koul, A.; Arnoult, E.; Lounis, N.; Guillemont, J. E. G.; Andries, K. The challenge of new drug discovery for tuberculosis. *Nature* **2011**, *469*, 483–490.
12. Check, E. After decades of drought, new drug possibilities flood TB pipeline. *Nat. Med.* **2007**, *13*, 266-266.
13. Dye, C. Doomsday postponed? Preventing and reversing epidemics of drug-resistant tuberculosis. *Nat. Rev. Microbiol.* **2009**, *7*, 81–87.
14. Zumla, A.; Nahid, P.; Cole, S. T. Advances in the development of new tuberculosis drugs and treatment regimens. *Nat. Rev.* **2013**, *12*, 388-404.
15. Lienhardt, C.; Vernon, A.; Raviglione, M. C. New drugs and new regimens for the treatment of tuberculosis: Review of the drug development pipeline and implications for national programmes. *Curr. Opin. Pulm. Med.* **2010**, *16*, 186–193.
16. Silver, L. L. Challenges of antibacterial discovery. *Clin. Microbiol. Rev.* **2011**, *24*, 71–109.
17. Andries, K.; Verhasselt, P.; Guillemont, J. E. G.; Gohlmann, H. W. H.; Neefs, J. M.; Winkler, H.; van Gestel, J.; Timmerman, P.; Zhu, M.; Lee, E.; Williams, P.; de Chaffoy, D.; Huitric, E.; Hoffner, S. E.; Cambau, E.; Truffot-Pernot, C.; Lounis, N.; Jarlier, V.
A diarylquinoline drug active on the ATP synthase of *Mycobacterium tuberculosis*. *Science* **2005**, *307*, 223–227.
18. Haagsma A. C.; Abdillahi-Ibrahim, R.; Wagner, M. J.; Krab, K.; Vergauwen, K.; Guillemont, J.; Andries, K.; Lill, H.; Koul, A.; Bald, D. Selectivity of TMC207 towards mycobacterial ATP synthase compared with that towards the eukaryotic homologue. *Antimicrob. Agents Chemother.* **2009**, *53*, 1290-1292.

19. Mdluli, K.; Kaneko, T.; Upton, A. The tuberculosis drug discovery and development pipeline and emerging drug targets. *Cold Spring Harb. Perspect. Med.* **2015**, 5:a021154
20. von Ballmoos, C.; Cook, G. M.; Dimroth, P. Unique rotary ATP synthase and its biological diversity. *Ann. Rev. Biophys.* **2008**, 37, 43–64.
21. Hong, S.; Pedersen, P. L. ATP Synthase and the actions of inhibitors utilized to study its roles in human health, disease, and other scientific areas. *Microbiol. Mol. biol. Rev.* **2008**, 72, 590–641.
22. Beechey, R. B.; Holloway, C. T.; Knight, I. G.; Robertson, A. M. Dicyclohexylcarbodiimide - An inhibitor of oxidative phosphorylation. *Biochem. Biophys. Res. Comm.* **1966**, 23, 76-80.
23. Matsuno-Yagi, A.; Hatefi, Y. Studies on the mechanism of oxidative phosphorylation. ATP synthesis by submitochondrial particles inhibited at Fo by venturicidin and organotin compounds. *J. Biol. Chem.* **1993a**, 268, 6186–6173.
24. Matsuno-Yagi, A.; Hatefi, Y. Studies on the mechanism of oxidative phosphorylation. Different effects of Fo inhibitors on unisite and multisite ATP hydrolysis by bovine submitochondrial particles. *J. Biol. Chem.* **1993b**, 268, 1539–1545.
25. Amacher, D. E. Drug-associated mitochondrial toxicity and its detection. *Curr. Med. Chem.* **2005**, 12, 1829–1839.
26. Wallace, K. B.; Starkov, A. A. Mitochondrial targets of drug toxicity. *Annu. Rev. Pharmacol. Toxicol.* **2000**, 40, 353–388.
27. Koul, A.; Vranckx, L.; Dendouga, N.; Balemans, W.; van den Wyngaert, I.; Vergauwen, K.; Gohlmann, H. W. H.; Willebrords, R.; Poncelet, A.; Guillemont, J.; Bald, D.;

- ACS Paragon Plus Environment

- H.; Jones, V.; Kim, Y. M.; Seo, M.; Seo, J. J.; Park, D.; Ko, Y.; Choi, I.; Kim, R.; Kim, S. Y.; Lim, S.; Yim, S. A.; Nam, J.; Kang, H.; Kwon, H.; Oh, C. T.; Cho, Y.; Jang, Y.; Chua, A.; Tan, B. H.; Nanjundappa, M. B.; Rao, S. P.; Barnes, W. S.; Wintjens, R.; Walker, J. R.; Alonso, S.; Lee, S.; Kim, J.; Oh, S.; Oh, T.; Nehrbass, U.; Han, S. J.; No, Z.; Lee, J.; Brodin, P.; Cho, S. N.; Nam, K.; Kim, J. Discovery of Q203, a potent clinical candidate for the treatment of tuberculosis. *Nat. Med.* **2013**, *19*, 1157-1160.
34. Khan, S. R.; Singh, S.; Roy, K. K.; Akhtar, M. S.; Saxena, A. K.; Krishnan, M. Y.; Biological evaluation of novel substituted chloroquinolines targeting mycobacterial ATP synthase. *Int. J. Antimicrob. Agents.* **2013**, *41*, 41-46.
35. Arora, K.; Ochoa-Montano, B.; Tsang, P. S.; Blundell, T. M.; Dawes, S. S.; Mizrahi, V.; Bayliss, T.; Mackenzie, C. J.; Cleghorn, L. A. T.; Ray, P. C.; Wyatt, P. G.; Uh, E.; Lee, J.; Barry III, C. E.; Boshoff, H. I. Respiratory flexibility in response to inhibition of cytochrome c oxidase in *Mycobacterium tuberculosis*. *Antimicrob. Agents chemother.* **2014**, *58*, 6962– 6965.
36. Chandraseker, N. S.; Alling, T.; Bailey, M. A.; Files, M.; Early, J. V.; Ollinger, J.; Ovechkina, Y.; Masquelin, T.; Desai, P. V.; Cramer, J. W.; Hipkind, P. A.; Odingo, J. O.; Parish, T. Identification of phenoxyalkylbenzimidazoles with antitubercular activity. *J. Med. Chem.* **2015**, *58*, 7273–7285.
37. Tantry, S. J.; Shinde, V.; Balakrishnan, G.; Markad, S. D.; Gupta, A. K.; Bhat, J.; Narayan, A.; Raichurkar, A.; Jena, L. K.; Sharma, S.; Kumar, N.; Nanduri, R.; Bharath, S.; Reddy, J.; Panduga, V.; Prabhakar, K. R.; Kandaswamy, K.; Kaur, P.; Dinesh, N.; Guptha, S.; Saralaya, R.; Panda, M.; Rudrapatna, S.; Mallya, M.; Rubin, H.; Yano, T.; Mdluli, K.; Cooper, C. B.; Balasubramanian, V.; Sambandamurthy, V. K.; Ramachandran, V.;

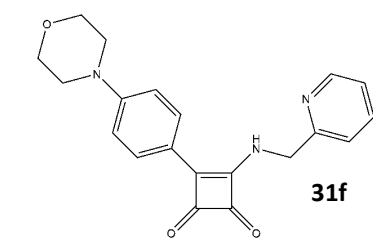
- Shandil, R. K.; Kavanagh, S.; Narayanan, S.; Iyer, P.; Mukherjee, K.; Hosagrahara, V. K.; Solapure, S.; Shahul Hameed P.; Ravishankar, S. Scaffold morphing led to evolution of 2,4-diaminoquinolines and aminopyrazolopyrimidines as inhibitors of ATP synthesis pathway. *Medchemcomm.* **2016**, 7, 1022 – 1032.
38. Alcaide, B.; Plumet, J.; Sierra, M. A.; Vicent, C. Reaction of arylglyoxals with 2-amino heterocycles. *J. Org. Chem.* **1989**, 54, 5763-5768.
39. Zheng, J.; Ramirez, V. D. Inhibition of mitochondrial proton FoF1-ATPase/ATP synthase by polyphenolic phytochemicals. *British J. Pharmacol.* **2000**, 130, 1115 – 1123.
40. Koul, A.; Dendouga, N.; Vergauwen, K.; Molenberghs, B.; Vranckx, L.; Willebrords, R.; Ristic, Z.; Lill, H.; Dorange, I.; Guillemont, J.; Bald, D.; Andries, K. Diarylquinolines target subunit c of mycobacterial ATP synthase. *Nat. Chem. Biol.* **2007**, 3, 323 -324.
41. Yano, T.; Kassovska-Bratinove, S.; The, J. S.; Winkler, J.; Sullivan, K.; Issacs, A.; Schechter, N. M.; Rubin, H. Reduction of clofazamine by mycobacterial type 2 NADH: quinone oxidoreductase. *J. Biol. Chem.* **2011**, 286, 10276-10287.
42. Hille, C.; Berg, M.; Bressel, L.; Munzke, D.; Primus, P.; Löhmannsröben, H. G.; Dosche, C. Time-domain fluorescence lifetime imaging for intracellular pH sensing in living tissues. *Anal. Bioanal. Chem.* **2008**, 391, 1871–1879.
43. Gentry, D. R.; Wilding, I.; Johnson, J. M.; Chen, D.; Remlinger, K.; Richards, C.; Neill, S.; Zalacain, M.; Rittenhouse, S. F.; Gwynn, M. N. A rapid microtiter plate assay for measuring the effect of compounds on *Staphylococcus aureus* membrane potential. *J. Microbiol. Methods* **2010**, 83, 254-256.
44. Segala, E.; Sougakoff, W.; Nevejans-Chauffour, A.; Jarlier, V.; Petrella, S. New mutations in the mycobacterial ATP synthase: New insights into the binding of the diarylquinoline

- TMC207 to the ATP synthase C-ring structure. *Antimicrob. Agents Chemother.* **2012**, *56*, 2326–2334.
45. Huitric, E.; Verhasselt, P.; Koul, A.; Andries, K.; Hoffner, S.; Andersson, D. I. Rates and mechanisms of resistance development in *Mycobacterium tuberculosis* to a novel diarylquinoline ATP synthase inhibitor. *Antimicrob. Agents Chemother.* **2010**, *54*, 1022–1028.
46. Preiss, L.; Langer, J. D.; Yildiz, Ö.; Eckhardt-Strelau, L.; Guillemont, J. E.; Koul, A.; Meier, T.; Structure of the mycobacterial ATP synthase Fo rotor ring in complex with the anti-TB drug bedaquiline. *Sci. Adv.* **2015**, *1*, e1500106.
47. Schrödinger Suite 2013-1, Induced fit docking protocol; Glide version 5.9, Prime version 3.2, Schrödinger, LLC, New York, NY, **2013**.
48. Schrödinger, version 9.4; Schrodinger, LLC: New York, **2013**.
49. Payne, D. J.; Gwynn, M. N.; Holmes, D. J.; Pompliano, D. L. Drugs for bad bugs: Confronting the challenges of antibacterial discovery. *Nat. Rev. Drug Discov.* **2007**, *6*, 29–40.
50. Balasubramanian, V.; Solapure, S.; Iyer, H.; Ghosh, A.; Sharma, S.; Kaur, P.; Deepthi, R.; Subbulakshmi, V.; Ramya, V.; Ramachandran, V.; Balganes, M.; Wright, L.; Melnick, D.; Butler, S. L.; Sambandamurthy, V. K. Bactericidal activity and mechanism of action of AZD5847, a novel oxazolidinone for treatment of tuberculosis. *Antimicrob. Agents Chemother.* **2014**, *58*, 495 - 502.
51. Shirude, P. S.; Shandil, R.; Sadler, C.; Naik, M.; Hosagrahara, V.; Hameed, S.; Shinde, V.; Bathula, C.; Humnabadkar, V.; Kumar, N.; Reddy, J.; Panduga, V.; Sharma, S.; Ambady, A.; Hegde, N.; Whiteaker, J.; McLaughlin, R. E.; Gardner, H.; Madhavapeddi, P.;

1
2
3
4
5
6
7
8
9
10
11
12
13
14
15
16
17
18
19
20
21
22
23
24
25
26
27
28
29
30
31
32
33
34
35
36
37
38
39
40
41
42
43
44
45
46
47
48
49
50
51
52
53
54
55
56
57
58
59
60

Ramachandran, V.; Kaur, P.; Narayan, A.; Guptha, S.; Awasthy, D.; Narayan, C.; Mahadevaswamy, J.; Vishwas, K. G.; Ahuja, V.; Srivastava, A.; Prabhakar, K. R.; Bharath, S.; Kale, R.; Ramaiah, M.; Choudhury, N. R.; Sambandamurthy, V. K.; Solapure, S.; Iyer, P. S.; Narayanan, S.; Chatterji, M. Azaindoles: Noncovalent DprE1 inhibitors from scaffold morphing efforts kill *Mycobacterium tuberculosis* and are efficacious *in vivo*. *J. Med. Chem.* **2013**, *56*, 9701–9708.

Table of Contents Graphic



Squaramide lead
Myc_ATPS IC₅₀ : 0.03 μ M
Mtb MIC: 0.5 μ M
Selectivity index: >1000
Effective against Bedaquiline resistant strain
Efficacious in vivo

